SIAM J. NUMER. ANAL.
Vol. 37, No. 3, pp. 827–862

THE EXPLICIT-JUMP IMMERSED INTERFACE METHOD: FINITE DIFFERENCE METHODS FOR PDES WITH PIECEWISE SMOOTH SOLUTIONS*

ANDREAS WIEGMANN† AND KENNETH P. BUBE‡

We dedicate this work to Helmut Rohrl on the occasion of his 70th birthday.

Abstract. Many boundary value problems (BVPs) or initial BVPs have nonsmooth solutions, with jumps along lower-dimensional interfaces. The explicit-jump immersed interface method (EJIIM) was developed following Li's fast iterative immersed interface method (FIIIM), recognizing that the foundation for the efficient solution of many such problems is a good solver for elliptic BVPs. EJIIM generalizes the class of problems for which FIIIM is applicable. It handles interfaces between constant and variable coefficients and extends the immersed interface method (IIM) to BVPs on irregular domains with Neumann and Dirichlet boundary conditions. Proofs of second order convergence for a one-dimensional (1D) problem with piecewise constant coefficients and for two-dimensional (2D) problems with singular sources are given. Other problems are reduced to the singular sources case, with additional equations determining the source strengths. The advantages of EJIIM are high quality of solutions even on coarse grids and easy adaptation to many problems with complicated geometries, while still maintaining the efficiency of the FIIIM.

Key words. elliptic boundary value problems, immersed interface method, Cartesian grid, nonsmooth solutions, irregular domain, interface, singular source, discontinuous coefficients, finite difference methods

AMS subject classifications. 65N06, 35R05, 31C20, 35J25, 65N22, 31A10

PII. S0036142997328664

1. Introduction.

Standard finite difference approximations fail when applied to nonsmooth functions because the Taylor expansions that they are based on are not valid. But many applications lead to nonsmooth solutions. These can be dealt with by adaptive methods, for example, by finite element methods, where element boundaries may be chosen to coincide with the interface, or by boundary fitted finite difference schemes. Considerable effort in constructing a grid has to be spent in these cases.

We concern ourselves with problems where this grid construction is not affordable, presumably because the location of the discontinuity is either not fixed (for example, in moving interface problems) or to be determined (as in inverse problems or in design problems). The discontinuities are assumed to occur along smooth, $n-1$ dimensional hypersurfaces, for example, simple closed curves in two dimensions. We approximate the solution on a uniform Cartesian grid on some domain in which the interfaces lie. Irregular domains are imbedded in rectangular domains, their boundaries being treated as interfaces. The key idea of EJIIM is to avoid grid generation by correcting the finite differences in the neighborhood of the interface. This fundamental idea of the IIM of using jumps in the solution and its derivatives in finite difference schemes on

*Received by the editors October 13, 1997; accepted for publication (in revised form) November 17, 1998; published electronically February 16, 2000. This work was supported in part by National Science Foundation grants DMS-9303404 and DMS-9626645 and Department of Energy grants DE-FG06-93ER25181 and DE-FG03-96ER25292.

http://www.siam.org/journals/sinum/37-3/32866.html

†Department of Mathematics, Lawrence Berkeley National Laboratory, Mail Stop 50A-2152, 1 Cyclotron Road, Berkeley, CA 94720 (wiegmann@math.lbl.gov).

‡University of Washington, Department of Mathematics, Box 354350, Seattle, WA 98195-4350 (bube@math.washington.edu).

uniform Cartesian grids originated with LeVeque and Li [4] and Li [5], building on the ideas of Peskin's immersed boundary method [10, 15]. The idea of correcting standard differences comes from Li [6], and corrections in the coordinate directions were already used by Mayo [8]. Two fundamental questions are, What is the nature of the singularity of the solution at an interface? and once that is determined, How can we introduce the singularity into a finite difference scheme?

We give an answer to the second question in one dimension in section 2, where we also prove convergence of EJIIM for a 1D problem with piecewise constant coefficients. Section 3 describes how to carry out EJIIM discretizations in two dimensions for the Laplacian and mixed derivatives. Then we answer the first question by stating jump conditions for various elliptic problems in section 4. Since some of these jump conditions involve jumps in the normal and tangential directions, in section 5 we give the transformations needed to derive the jumps in the Cartesian coordinate directions as required in section 2. Section 6 contains a second order convergence proof for known jumps and completes the derivation of finite difference schemes via one-sided differences for the various problems with unknown jumps stated in section 4. Finally, in section 7, we show some numerical examples comparing EJIIM with IIM [4] and Li's FIIIM [6] and also some examples applying EJIIM to interior and exterior BVPs on irregular domains.

2. EJIIM theory in one dimension. How can we modify standard differences, for example, the $O(h^2)$ approximations

$$u_x(x_i, y_j) \approx \frac{u(x_{i+1}, y_j) - u(x_{i-1}, y_j)}{2h}, \tag{1}$$

$$\Delta u(x_i, y_j) \approx \frac{u(x_{i+1}, y_j) + u(x_{i-1}, y_j) + u(x_i, y_{j+1}) + u(x_i, y_{j-1}) - 4u(x_i, y_j)}{h^2}, \tag{2}$$

in the case that an interface cuts through the stencil used by the differences? For EJIIM, following Mayo [8], the answer lies in 1 dimension. To denote jumps in a function u and its derivatives at a point α, we write

$$[u^{(m)}]_\alpha = \lim_{x \to \alpha^+} u^{(m)}(x) - \lim_{x \to \alpha^-} u^{(m)}(x);$$

in short, $[.] = [.]_\alpha$. As usual, by $u^{(0)}$ we mean the function u itself.

2.1. Correcting finite differences with known jumps. We start with a lemma where the interface occurs at $\alpha = 0$, which lies between two arbitrarily located grid points (labeled here h^- and h^+) with grid spacing h.

LEMMA 1. *Assume $u^- \in C^{l+1}[-1, 0]$ and $u^+ \in C^{l+1}[0, 1]$. Let $\alpha = 0$ and*

$$u = \begin{cases} u^-(x) & \text{for } x \le 0, \\ u^+(x) & \text{for } x > 0. \end{cases}$$

Then for $h < 1$ and any h^- and $h^+ = h^- + h$ satisfying $-h < h^- \le 0 < h^+$,

$$\left| u(h^+) - \sum_{k=0}^{l} \frac{h^k}{k!} u^{(k)}(h^-) - \sum_{k=0}^{l} \frac{(h^+)^k}{k!} [u^{(k)}] \right| \le \frac{K}{(l+1)!} h^{l+1},$$

where

$$K = \max \left(\max_{x \in [-1,0]} \left| (u^-)^{(l+1)}(x) \right|, \max_{x \in [0,1]} \left| (u^+)^{(l+1)}(x) \right| \right)$$

is sharp.

Proof. A Taylor expansion for u^+ at 0 yields

$$u(h^+) = \sum_{m=0}^{l} \frac{(h^+)^m}{m!}(u^+)^{(m)}(0) + \frac{(u^+)^{(l+1)}(\xi_{l+1})}{(l+1)!}(h^+)^{l+1}$$

for some $\xi_{l+1} \in (0, h^+)$. Also, $(u^+)^{(m)}(0) = (u^-)^{(m)}(0) + [u^{(m)}]$, and hence

$$u(h^+) = \sum_{m=0}^{l} \frac{(h^+)^m}{m!}\left\{(u^-)^{(m)}(0) + [u^{(m)}]\right\} + \frac{(u^+)^{(l+1)}(\xi_{l+1})}{(l+1)!}(h^+)^{l+1}.$$

Taylor expansions for u^- at h^- yield for $m = 0, 1, \ldots, l$

$$(u^-)^{(m)}(0) = \sum_{j=0}^{l-m} \frac{(-h^-)^j}{j!}(u^-)^{(j+m)}(h^-) + \frac{(u^-)^{(l+1)}(\xi_m)}{(l-m+1)!}(-h^-)^{l-m+1}$$

for some $\xi_m \in (h^-, 0)$. Since u agrees with u^- in a (left-sided) neighborhood of zero,

$$u(h^+) = \sum_{m=0}^{l} \frac{(h^+)^m}{m!}\left\{[u^{(m)}] + \sum_{j=0}^{l-m} \frac{(-h^-)^j}{j!}u^{(j+m)}(h^-)\right\} + \frac{(u^+)^{(l+1)}(\xi_{l+1})}{(l+1)!}(h^+)^{l+1} + \sum_{m=0}^{l} \frac{(h^+)^m}{m!}\frac{(u^-)^{(l+1)}(\xi_m)}{(l-m+1)!}(-h^-)^{l-m+1}.$$

Changing the order of summation ($k = m + j$, so $j = k - m$),

$$u(h^+) - \sum_{k=0}^{l}\left\{\frac{(h^+)^k}{k!}[u^{(k)}] + \left\{\sum_{m=0}^{k} \frac{(-h^-)^{k-m}}{(k-m)!}\frac{(h^+)^m}{m!}\right\}u^{(k)}(h^-)\right\} = \sum_{m=0}^{l+1} \frac{(h^+)^m}{m!}\frac{(u^\pm)^{(l+1)}(\xi_m)}{(l-m+1)!}(-h^-)^{l-m+1},$$

where $u^\pm = u^-$ for $m = 0, 1, \ldots, l$ and $u^\pm = u^+$ for $m = l + 1$. Finally, the desired result follows from the binomial theorem, the facts that $h = h^+ - h^-$, $0 \le -h^- < h$, $0 < h^+ \le h$, and simple estimates. The piecewise linear example $u = |x|$ with $l = 0$ shows that K is sharp. ∎

REMARK 2. *On the other side of the interface, the expansion formula is*

$$u(h^-) = \sum_{k=0}^{l} \frac{(-h)^k}{k!}u^{(k)}(h^+) - \sum_{k=0}^{l} \frac{(h^-)^k}{k!}[u^{(k)}] + O\left(h^{l+1}\right).$$

The "−" for the second sum is introduced by the "nonsymmetric" definition of $[u^{(k)}]$.

Next, we apply Lemma 1 to the situation where the interface lies at an arbitrary location between two grid points x_j and $x_{j+1} = x_j + h$.

LEMMA 3 (jump-corrected differences). *Let $x_j \le \alpha < x_{j+1}$, $h^- = x_j - \alpha$, and $h^+ = x_{j+1} - \alpha$. Suppose $u \in C^4[x_j - h, \alpha) \cap C^4(\alpha, x_{j+1} + h]$, with derivatives extending continuously up to the boundary α. Then the following approximations hold to $O(h^2)$:*

$$u_x(x_j) \approx \frac{u(x_{j+1}) - u(x_{j-1})}{2h} - \frac{1}{2h} \sum_{m=0}^{2} \frac{(h^+)^m}{m!} [u^{(m)}], \tag{3}$$

$$u_x(x_{j+1}) \approx \frac{u(x_{j+2}) - u(x_j)}{2h} - \frac{1}{2h} \sum_{m=0}^{2} \frac{(h^-)^m}{m!} [u^{(m)}], \tag{4}$$

$$u_{xx}(x_j) \approx \frac{u(x_{j+1}) - 2u(x_j) + u(x_{j-1})}{h^2} - \frac{1}{h^2} \sum_{m=0}^{3} \frac{(h^+)^m}{m!} [u^{(m)}], \tag{5}$$

$$u_{xx}(x_{j+1}) \approx \frac{u(x_{j+2}) - 2u(x_{j+1}) + u(x_j)}{h^2} + \frac{1}{h^2} \sum_{m=0}^{3} \frac{(h^-)^m}{m!} [u^{(m)}]. \tag{6}$$

Proof. (i) Formulas (3), (5): By shifting the coordinate system by $-\alpha$ we are in the regime of Lemma 1. The formulas follow by using Lemma 1 for $u(x_{j+1}) = u(h^+)$ and the usual Taylor expansions for $u(x_j) = u(h^-)$ and $u(x_{j-1}) = u(h^- - h)$. The signs on the corrections are the same because $u(x_{j+1})$ occurs with a positive sign in both difference approximations.

(ii) Formulas (4), (6): The formulas follow by using Remark 2 for $u(x_j) = u(h^-)$ and the usual Taylor expansions for $u(x_{j+1}) = u(h^+)$ and $u(x_{j+2}) = u(h^+ + h)$. The signs on the corrections differ because $u(x_j)$ occurs in (6) with a positive sign but with a negative sign in (4). ∎

The same ideas extend to multiple interfaces.

LEMMA 4 (multiple corrections). (a) *Let $x_{j-1} \le \alpha_1 < x_j \le \alpha_2 < x_{j+1}$, $h_1^- = x_{j-1} - \alpha_1$, $h_1^+ = x_j - \alpha_1$, $h_2^- = x_j - \alpha_2$, and $h_2^+ = x_{j+1} - \alpha_2$. Suppose $u \in C^4[x_{j-1}, \alpha_1) \cap C^4(\alpha_1, \alpha_2) \cap C^4(\alpha_2, x_{j+1}]$, with derivatives extending continuously up to the boundaries of the subintervals. Then the following approximations hold to $O(h^2)$:*

$$u_x(x_j) \approx \frac{u(x_{j+1}) - u(x_{j-1})}{2h} - \frac{1}{2h} \sum_{m=0}^{2} \frac{(h_1^-)^m [u^{(m)}]_{\alpha_1} + (h_2^+)^m [u^{(m)}]_{\alpha_2}}{m!}, \tag{7}$$

$$u_{xx}(x_j) \approx \frac{u(x_{j+1}) - 2u(x_j) + u(x_{j-1})}{h^2} + \frac{1}{h^2} \sum_{m=0}^{3} \frac{(h_1^-)^m [u^{(m)}]_{\alpha_1} - (h_2^+)^m [u^{(m)}]_{\alpha_2}}{m!}. \tag{8}$$

(b) *Let $x_j \le \alpha_1 < \alpha_2 < x_{j+1}$, $h_1^- = x_j - \alpha_1$, $h_1^+ = x_{j+1} - \alpha_1$, $h_2^- = x_j - \alpha_2$, and $h_2^+ = x_{j+1} - \alpha_2$. Suppose $u \in C^4[x_j, \alpha_1) \cap C^4(\alpha_1, \alpha_2) \cap C^4(\alpha_2, x_{j+1}]$, with derivatives extending continuously up to the boundaries. Then the following approximations hold*

to $O(h^2)$*:*

$$u_x(x_j) \approx \frac{u(x_{j+1}) - u(x_{j-1})}{2h} - \frac{1}{2h}\sum_{m=0}^{2} \frac{(h_1^+)^m[u^{(m)}]_{\alpha_1} + (h_2^+)^m[u^{(m)}]_{\alpha_2}}{m!},$$

$$u_x(x_{j+1}) \approx \frac{u(x_{j+2}) - u(x_j)}{2h} - \frac{1}{2h}\sum_{m=0}^{2} \frac{(h_1^-)^m[u^{(m)}]_{\alpha_1} + (h_2^-)^m[u^{(m)}]_{\alpha_2}}{m!},$$

$$u_{xx}(x_j) \approx \frac{u(x_{j+1}) - 2u(x_j) + u(x_{j-1})}{h^2} - \frac{1}{h^2}\sum_{m=0}^{3} \frac{(h_1^+)^m[u^{(m)}]_{\alpha_1} + (h_2^+)^m[u^{(m)}]_{\alpha_2}}{m!},$$

$$u_{xx}(x_{j+1}) \approx \frac{u(x_{j+2}) - 2u(x_{j+1}) + u(x_j)}{h^2} + \frac{1}{h^2}\sum_{m=0}^{3} \frac{(h_1^-)^m[u^{(m)}]_{\alpha_1} + (h_2^-)^m[u^{(m)}]_{\alpha_2}}{m!}.$$

Proof. In either case (a) or (b) apply Lemma 1 twice. ∎

REMARK 5. *If* $\alpha = x_j$ *in Lemma* 3 *or* $\alpha_1 = x_{j-1}$ *or* $\alpha_2 = x_j$ *in Lemma* 4*, values of* u *and derivatives on* u *at these points indicate left-sided limits.*

2.2. Convergence for piecewise constant coefficients. Now we consider a simple problem with discontinuous coefficients. β is piecewise constant and there exists a single interface point α with $0 < \alpha < 1$, such that β and possibly f are discontinuous at α, but continuous on $[0, \alpha)$ and $(\alpha, 1]$.

$$\frac{d}{dx}\left(\beta(x)\frac{du(x)}{dx}\right) = f(x), \tag{9}$$

$$u(0) = u_l, \tag{10}$$

$$u(1) = u_r. \tag{11}$$

In order even to write the equation we have to assert that u and βu_x are continuous. From this we may derive formulas for the jumps:

$$[u] = 0, \tag{12}$$

$$[u_x] = \left(\frac{\beta^-}{\beta^+} - 1\right) u_x^-, \tag{13}$$

$$[u_{xx}] = \left[\frac{f}{\beta}\right], \tag{14}$$

$$[u_{xxx}] = \left[\frac{f_x}{\beta}\right]. \tag{15}$$

The first, third, and fourth jumps are known and fall within the framework of the previous section. But the second jump[1] depends on the solution.[2] Finding this jump is part of the numerical solution process. This motivates us to introduce the unknown jump as an additional variable, g_1. Making the jumps explicit allows us to simplify (9):

$$u_{xx} = \frac{f}{\beta}. \tag{16}$$

[1] We could also have written $[u_x]$ as a function of u_x^+. The formulas for the jumps are not unique and may even involve different order derivatives in different formulas for the same jump.

[2] This is the main difficulty for this problem. The case when all jumps are known is easier; we give it later in two dimensions.

We discretize the interval $[0,1]$ with $n+1$ uniformly spaced points (meshwidth $h = 1/n$), $x_i = i/n$, $i = 0, 1, 2, \ldots, n$. As before, j is chosen so that $x_j \le \alpha < x_{j+1}$. Known jumps enter the discretization as simply correcting the right-hand side of the linear system resulting from a standard centered difference discretization of (16), using the formulas from the previous section. The unknown jump g_1 is corrected in the same fashion as known jumps, but in addition we need an equation for its value. For the problem under consideration, this equation is a discretization of (13). We approximate (13) simply using one-sided interpolation to the interface point.

We write this out as a linear system, emphasizing the block structure. The vector U contains the grid variables located at $x_1, x_2, \ldots, x_{n-1}$ and the discretization of (16) is written above the discretization of (13).[3]

$$\left[\begin{array}{c|c} \mathcal{A}_1 & -\Psi_1 \\ \hline D^T & 1 \end{array}\right] \left[\begin{array}{c} U \\ \hline g_1 \end{array}\right] = \left[\begin{array}{c} F + B + \left[\frac{f}{\beta}\right] \Psi_2 \\ \hline 0 \end{array}\right], \tag{17}$$

where

$$\mathcal{A}_1 = \frac{1}{h^2} \begin{bmatrix} -2 & 1 & & & \\ 1 & -2 & 1 & & \\ & \ddots & \ddots & \ddots & \\ & & 1 & -2 & 1 \\ & & & 1 & -2 \end{bmatrix} \tag{18}$$

is a discretization of the Laplacian with zero Dirichlet boundary conditions,

$$F = \left[\frac{f(x_1)}{\beta(x_1)}, \frac{f(x_2)}{\beta(x_2)}, \ldots, \frac{f(x_{n-1})}{\beta(x_{n-1})}\right]^T, \text{ and} \tag{19}$$

$$B = \left[\frac{-u_l}{h^2}, 0, 0, \ldots, 0, \frac{-u_r}{h^2}\right]^T \tag{20}$$

are the discretization of the right-hand side and boundary conditions,[4] and

$$D^T = -\left(\frac{\beta^-}{\beta^+} - 1\right) \frac{1}{2h^2} [0, \ldots, 0, -2h^- + h, 4h^- - 4h, \underbrace{-2h^- + 3h}_{j\text{th entry}}, 0, \ldots, 0] \tag{21}$$

performs one-sided interpolation of the derivative on a vector of grid values to the interface α to $O(h^2)$ and multiplies this value with the constant required from (13). The vectors

$$\Psi_1 = \left[0, 0, \ldots, 0, \frac{h^+}{h^2}, -\frac{h^-}{h^2}, 0, 0, \ldots, 0\right]^T, \tag{22}$$

$$\Psi_2 = \left[0, 0, \ldots, 0, \frac{{h^+}^2}{2h^2}, -\frac{{h^-}^2}{2h^2}, 0, 0, \ldots, 0\right]^T \tag{23}$$

[3] This assumes $1 > \alpha \ge 3h$. In case $3h > \alpha > 0$, the other equation (see footnote 1 on the previous page) for $[u_x]$ should be utilized. This results in a change in the definition of D^T and small modifications in what follows.

[4] The boundary conditions enter the discretization in a singular way intimately related to the EJIIM. This is elaborated on in [16].

represent the coefficients of the jumps in Lemma 1, introduced in the appropriate equations.

The system (17) uses jumps only up to the second derivatives. This means that the truncation error at x_j and x_{j+1} is $O(h)$, not $O(h^2)$. We now prove quadratic convergence even in the presence of a locally larger truncation error. This behavior was already observed for numerical examples in [4].

THEOREM 6 (EJIIM convergence for piecewise constant coefficients). *Consider the BVP* (9)–(11)*, where β is piecewise constant, i.e.,*

$$\beta = \begin{cases} \beta^- & \text{for } 0 \le x < \alpha, \\ \beta^+ & \text{for } \alpha < x \le 1. \end{cases}$$

With second order corrections, EJIIM finds approximate solutions U so that

$$\|Eu - U\|_\infty = O(h^2).$$

The proof of Theorem 6 is based on the second Schur-complement of (17) and will be stated after a sequence of auxiliary lemmas. For convenience of notation, we write $\rho = \beta^-/\beta^+$, $\Psi \equiv \Psi_1$, $F_1 \equiv F + B + \left[\frac{f}{\beta}\right]\Psi_2$ and for generality $0 = F_2$. Then $\mathcal{A}_1 U - \Psi g_1 = F_1$ and $D^T U + g_1 = F_2$, and hence

$$\left(\mathcal{A}_1 + \Psi D^T\right) U = F_1 + \Psi F_2.$$

This is a system involving only the approximate solution after eliminating the jump variable. First, we collect useful properties of $\mathcal{A}_1$ that by themselves suffice for an easy convergence proof for the smooth version of Theorem 6.

LEMMA 7. *The (i,j) entry of $\mathcal{A}_1^{-1} \in \mathbf{R}^{(n-1)\times(n-1)}$ (for $n > 3$) is*

$$a_{ij} = \frac{\min(i,j)\,(\max(i,j) - n)}{n^3}.$$

Proof. Check that the proposed "inverse" does the job. ∎

LEMMA 8. *$\|\mathcal{A}_1^{-1}\|_\infty = 1/8$ for n even and $\|\mathcal{A}_1^{-1}\|_\infty = (1 - n^{-2})/8$ for n odd.*

Proof. For the two cases n even and n odd, first we show that $\sum_j |a_{ij}|$ has the desired value for some i, then we show that this value is the maximum. We rely heavily on the explicit formulas given in Lemma 7.

For n even, row $n/2$ has entries

$$\frac{1}{2n^2}\left\{-1, -2, -3, \dots, \frac{-n}{2}, \frac{2-n}{2}, \frac{4-n}{2}, \dots, \frac{-2}{2}\right\}.$$

The absolute values sum up as

$$\sum_{j=1}^{n-1} \left|a_{\frac{n}{2}j}\right| = \frac{1}{n^3}\left\{\frac{n}{2}\sum_{j=1}^{\frac{n}{2}-1} 2j + \frac{n^2}{4}\right\} = \frac{1}{n^3}\left\{\frac{n^3}{8} - \frac{n^2}{4} + \frac{n^2}{4}\right\} = \frac{1}{8}.$$

Consider row i, with $i < \frac{n}{2}$. For columns $j = 1, 2, \dots, i-1$, we find $|a_{i+1,j}| = |a_{i,j}| - j$. But for columns $j = i, i+1, \dots, n-1$, we find $|a_{i+1,j}| = |a_{i,j}| + n - j$. Since there are more columns of the latter type, the absolute row sums increase:

$$\sum_{j=1}^{n-1} |a_{i+1,j}| - \sum_{j=1}^{n-1} |a_{i,j}| \ge n - i > 0.$$

For row i with $i \geq \frac{n}{2}$, there are more columns of the first type, which yields that the absolute row sum decreases from row i to row $i+1$, finishing the argument for the case where n is even. For n odd, rows $\frac{n-1}{2}$ and $\frac{n+1}{2}$ have the entries (for row $\frac{n+1}{2}$ up to permutation)

$$\frac{1-n}{2n^3}\left\{-\frac{n+1}{1-n}, -2\left(\frac{n+1}{1-n}\right), -3\left(\frac{n+1}{1-n}\right), \ldots, \frac{n+1}{2}, \frac{n-1}{2}, \frac{n-3}{2}, \ldots, 1\right\}.$$

The absolute values sum up as

$$\sum_{j=1}^{n-1}\left|a_{\frac{n-1}{2}j}\right| = \frac{1}{n^3}\sum_{j=1}^{\frac{n-1}{2}}\left\{\frac{n+1}{2}+\frac{n-1}{2}\right\}j = \frac{1}{n^3}\frac{n^3-n}{8} = \frac{1-n^{-2}}{8}.$$

The proof that these two rows attain the maximum absolute row sum is analogous to the case where n is even, with the exception that here two rows attain that maximum and we need to consider the cases $i < \frac{n-1}{2}$ and $i \geq \frac{n+1}{2}$. ∎

In the case that $\beta = 1$ and f is smooth, the discretization reduces to

$$\mathcal{A}_1 U = F + B.$$

The truncation error T measures how well the evaluation of the exact solution on the grid points, Eu, satisfies the discrete system.

$$\mathcal{A}_1 Eu = F + B + T,$$

here $T = O(h^2)$ in the ∞-norm. We find $Eu - U = \mathcal{A}_1^{-1}T$ and

$$\|Eu - U\|_\infty = \|\mathcal{A}_1^{-1}T\|_\infty \leq \|\mathcal{A}_1^{-1}\|_\infty \|T\|_\infty = \|\mathcal{A}_1^{-1}\|_\infty O(h^2). \tag{24}$$

Lemma 8 gives $\|\mathcal{A}_1^{-1}\|_\infty \leq K$ independent of n, yielding second order convergence in the smooth case.

PROPOSITION 9 (local truncation error). *Equation* (17) *discretizes the jump to second order,*

$$D^T U = [u_x] + O\left(h^2\right).$$

Away from α*, that is, for* $i \notin \{j, j+1\}$*, the local truncation error of* (17) *is* $O\left(h^2\right)$*,*

$$\left|(\mathcal{A}_1 Eu - \Psi g - F_1)_i\right| = O\left(h^2\right).$$

Near the interface, that is, for $i \in \{j, j+1\}$*, it suffices to discretize* g_1 *to second order,* $g_1 = [u_x] + O\left(h^2\right)$*, to achieve* $O(h)$ *local truncation error of the* i*th equation in* (17)*,*

$$\left|(\mathcal{A}_1 Eu - \Psi g - F_1)_i\right| = O(h).$$

Proof. The first property holds by design of D^T as interpolating the first derivative of a second-degree polynomial through the points (x_{j-2}, U_{j-2}), (x_{j-1}, U_{j-1}), and (x_j, U_j), then multiplying the result by $(1-\rho)$.

For $i \notin \{j, j+1\}$ the standard centered differences for d^2/dx^2 are $O\left(h^2\right)$, and $(\Psi g)_i = 0$. So the restriction Eu to the grid of a solution u of (16) satisfies (17) to $O\left(h^2\right)$, since $(\mathcal{A}_1 Eu)_i = u_{xx}(x_i) + O\left(h^2\right)$, and $u_{xx}(x_i) = f(x_i)/\beta(x_i)$.

For $i = j$, the proposed accuracy of g_1 when replacing $[u_x]$ in (5) makes (5) an $O(h)$ approximation to $u_{xx}(x_j)$, which yields the claim. The same argument can be used for $i = j + 1$. ∎

The following very useful result is found for example in the book by Golub and Van Loan [2].

LEMMA 10 (Sherman–Morrison–Woodbury formula).

$$\left(\mathcal{A}_1 + \Psi D^T\right)^{-1} = \mathcal{A}_1^{-1} - \mathcal{A}_1^{-1}\Psi\left(1 + D^T\mathcal{A}_1^{-1}\Psi\right)^{-1} D^T\mathcal{A}_1^{-1}. \tag{25}$$

Proof. Recall that $\mathcal{A}_1^{-1}$ exists by Lemma 7 and check that the proposed "inverse" does the job. ∎

As in the proof for the smooth problem we want $\| \left(\mathcal{A}_1 + \Psi D^T\right)^{-1} \|_\infty \le K$, with K independent of n. First we define the Green's kernel for the interval $[0, 1]$:

$$G(\alpha, x) = \begin{cases} (\alpha - 1)\, x, & 0 \le x \le \alpha, \\ (x - 1)\, \alpha, & \alpha < x \le 1. \end{cases} \tag{26}$$

It satisfies $\partial^2 G(\alpha, x)/\partial x^2 = \delta(x - \alpha)$ with $G(\alpha, 0) = G(\alpha, 1) = 0$ for all $\alpha \in (0, 1)$. The Green's kernel is symmetric and negative everywhere in $\Omega \times \Omega$.

The main insight is that Ψ is a "discrete delta-function" supported in $(\alpha - h, \alpha + h)$, and application of $\mathcal{A}_1^{-1}$ is "discrete integration" against a "discrete Green's kernel." This is made rigorous in the following lemma.

LEMMA 11 (discrete Green's kernel). *The kth entry of* $\mathcal{G}^\alpha \equiv \mathcal{A}_1^{-1}\Psi$ *satisfies*

$$\mathcal{G}_k^\alpha = \begin{cases} (\alpha - 1)\, hk, & 0 \le hk \le \alpha, \\ (hk - 1)\, \alpha, & \alpha < hk \le 1. \end{cases}$$

Proof. Instead of using $\mathcal{A}_1^{-1}$ explicitly, it is easier to verify that $\mathcal{A}_1\mathcal{G}^\alpha = \Psi$. ∎

COROLLARY 12. $\|\mathcal{A}_1^{-1}\Psi\|_\infty \le (1 - \alpha)\alpha$.

Proof. Use Lemma 11. ∎

The entries in $\mathcal{G}^\alpha$ are exactly the values of the Green's kernel on the grid. That is, the following diagram commutes for all h and all α:

$$\begin{array}{ccc} \delta(x - \alpha) & \xrightarrow{\text{"discretization"}} & \Psi \\ \text{integration against } G(\cdot, y)\Big\downarrow & \diagup \quad \diagup \quad \diagup & \Big\downarrow \text{application of } \mathcal{A}_1^{-1} \\ G(\alpha, y) & \xrightarrow[\text{discretization via } E]{} & \mathcal{G}^\alpha \end{array}$$

REMARK 13. *Furthermore, not surprising given the interpolation properties of* Ψ (*see* [16]), *for* $\alpha = x_i$, $h\mathcal{G}_k^{x_i}$ *is just the* kth *entry in the* ith *row of* $\mathcal{A}_1^{-1}$. *The* h *makes sense as well, representing "integration." This is an observation similar to one made in the proof of Lemma* 5.1 *in* [1].

LEMMA 14 (discrete integration of a difference functional). *The kth entry of* $\mathcal{D} \equiv \mathcal{A}_1^{-1}D$ *satisfies*

$$\mathcal{D}_k = (1 - \rho)\begin{cases} h^2 k, & k \le j - 2, \\ h^2 k + \frac{h}{2} - h^-, & k = j - 1, \\ h^2 k - h, & k \ge j, \end{cases}$$

where $x_j \le \alpha < x_{j+1}$ *defines* j *as usual.*

Proof. Instead of using $\mathcal{A}_1^{-1}$ explicitly, it is easier to verify that $\mathcal{A}_1\mathcal{D} = D$. ∎

COROLLARY 15. $\|\mathcal{A}_1^{-1}D\|_\infty \le \frac{5}{2n}\,|\rho - 1|$.

Proof. Take the maximum of the entries in $\mathcal{D}$ for all possible values of α. ∎

COROLLARY 16. $D^T\mathcal{A}_1^{-1}\Psi = (\alpha-1)(1-\rho) \quad (\in \mathbf{R})$.

Proof. Use the symmetry of $\mathcal{A}_1^{-1}$ (which implies that $D^T\mathcal{A}_1^{-1} = \mathcal{D}^T$) and the definition of Ψ. ∎

COROLLARY 17. *$\mathcal{A}_1 + \Psi D^T$ is invertible for all $\rho > 0$ and all $\alpha \in (0,1)$.*

Proof. By Lemma 10 it suffices to show that $1 + D^T\mathcal{A}_1^{-1}\Psi \neq 0$. But for this term we may use Corollary 16. For $0 < \rho \le 1$, $(\alpha-1)(1-\rho) > -1$, and for $\rho > 1$, $(\alpha-1)(1-\rho) > 1$. So $1 + (\alpha-1)(1-\rho) > 0$ for both cases. ∎

LEMMA 18 (sup norm bound for rank 1 matrices). *Let $u, v \in \mathbf{R}^{n-1}$; then*

$$\|uv^T\|_\infty \le (n-1)\,\|u\|_\infty\,\|v\|_\infty.$$

Proof. In the absolute row sums, bound all entries u_i, v_i by $\|u\|_\infty$, $\|v\|_\infty$, respectively. ∎

PROPOSITION 19. *For any matrices A, B, and any vectors e_1, e_2, the following holds:*

$$\begin{aligned}\|(A+B)(e_1+e_2)\|_\infty &\le \|(A+B)e_1\|_\infty + \|(A+B)e_2\|_\infty \\ &\le (\|A\|_\infty + \|B\|_\infty)\|e_1\|_\infty + \|Ae_2\|_\infty + \|Be_2\|_\infty.\end{aligned}$$

Proof. Matrix and vector norm properties. ∎

Proof of Theorem 6. By Proposition 9 the truncation error T satisfies

$$\left(\mathcal{A}_1 + \Psi D^T\right)(U - Eu) = T = T_1 + T_2,$$

where $\|T_1\|_\infty = O(h^2)$ and $\|T_2\|_\infty = O(h)$. The j and $j+1$ entries of T_1 are zero, and T_2 has only two nonzero entries: $(h^-/h - 1/3 - (h^-/h)^2/2)(1-\rho)u^-_{xxx}h^\pm + O\big(h^2\big)$, with h^+ corresponding to x_j and h^- corresponding to x_{j+1}. Using Lemma 10 and Proposition 19 with

$$A \equiv \mathcal{A}_1^{-1} \;\text{ and }\; B \equiv -\mathcal{A}_1^{-1}\Psi\left(I + D^T\mathcal{A}_1^{-1}\Psi\right)^{-1} D^T\mathcal{A}_1^{-1},$$

we will show (i) $\|\left(\mathcal{A}_1 + \Psi D^T\right)^{-1} T_1\|_\infty = O(h^2)$ and (ii) $\|\left(\mathcal{A}_1 + \Psi D^T\right)^{-1} T_2\|_\infty = O(h^2)$, which proves the theorem.

(i) From Lemma 8 we know that $\frac{1}{8} \sim \|A\|_\infty \le K_1$, and for B we see from Lemma 18 and the preceding corollaries that

$$\|\mathcal{A}_1^{-1}\Psi\left(I + D^T\mathcal{A}_1^{-1}\Psi\right)^{-1} D^T\mathcal{A}_1^{-1}\|_\infty \le \frac{n(1-\alpha)\alpha}{(1-(1-\alpha)(1-\rho))}\;\frac{5}{2n}\;|\rho - 1| = K_2.$$

Hence $\|\left(\mathcal{A}_1 + \Psi D^T\right)^{-1} T_1\|_\infty \le (K_1 + K_2)\|T_1\|_\infty = O(h^2)$.

(ii) To be precise, $T_2 = O(h)e_j + O(h)e_{j+1}$ where e_l is a unit vector with the lth entry equal to one. From Lemma 7 we find $\|\mathcal{A}_1^{-1}e_l\|_\infty \le \sup_i |a_{il}| = O(h)$. Similarly,

$$\begin{aligned}\|\mathcal{A}_1^{-1}\Psi\left(I + D^T\mathcal{A}_1^{-1}\Psi\right)^{-1} D^T\mathcal{A}_1^{-1}e_l\|_\infty &\le \|\mathcal{A}_1^{-1}\Psi\|_\infty \left|I + D^T\mathcal{A}_1^{-1}\Psi\right|^{-1} \left|D^T\mathcal{A}_1^{-1}e_l\right| \\ &\le \frac{(1-\alpha)\alpha}{1-(1-\alpha)(1-\rho)}\|D^T\mathcal{A}_1^{-1}\|_\infty \\ &\le \frac{(1-\alpha)\alpha}{1-(1-\alpha)(1-\rho)}\frac{5}{2n}|\rho - 1| \\ &= K_2 h = O(h)\,. \qquad ∎\end{aligned}$$

COROLLARY 20. *The numerical results found with EJIIM for varying α on a fixed grid can be compared:*[5]

$$\|Eu - U\|_\infty < \left(\frac{5}{2} + \frac{1}{4}\right)(\|T_1\|_\infty + \|T_2\|_\infty h)\,.$$

Proof. We only need to show that the bounds in Theorem 6 are uniform in the geometry and coefficient. For use in both (i) and (ii) in the proof of Theorem 6, there exists a uniform bound on K_2 for all $\rho > 0$ and $0 < \alpha < 1$. For $\rho > 1$,

$$\frac{5|\rho - 1|(1-\alpha)\alpha}{2 - 2(1-\alpha)(1-\rho)} < \frac{5(\rho-1)(1-\alpha)\alpha}{2(1-\alpha)(\rho-1)} < 5\alpha/2 < 5/2,$$

and for $0 < \rho \le 1$,

$$\frac{5|\rho - 1|(1-\alpha)\alpha}{2 - 2(1-\alpha)(1-\rho)} < \frac{5(1-\alpha)\alpha}{2 - 2(1-\alpha)} < 5\alpha/2 < 5/2.$$

Using Proposition 19 as in the proof of Theorem 6, this yields the uniform error bounds. ∎

REMARK 21. *It is clear that using third order jumps does not improve the asymptotic order of the error. Their usefulness lies in the improved smoothness of the error, and in allowing the construction of higher than second order methods, when a higher quality of the discretization near the interface is necessary.*

REMARK 22. *The truncation error T_2 determines the quality of the solution in the following sense: If the geometry is such that either $[u_x] = (\rho-1)u_x^-$ or $[u_x] = (1/\rho - 1)u_x^+$ could be used, then one should do finite differences after estimating and comparing $|(\rho-1)u_{xxx}^-|$ and $|(1/\rho-1)u_{xxx}^+|$. If u_{xxx}^- and u_{xxx}^+ are comparable, this comes down to discretizing $[u_x] = (\rho-1)u_x^-$ if $\rho < 1$ and $[u_x] = (1/\rho - 1)u_x^+$ if $\rho > 1$.*

3. EJIIM for the Laplacian and for cross derivatives. Lemma 1 is also the basis for correcting finite differences in higher dimensions. In 2D, let a smooth interface $\Gamma = \vec{X}(t) = (x(t), y(t))$ be parameterized by arclength t. In the case of a closed curve, let Γ be oriented in the positive direction, with the bounded domain on the left; in this case $\vec{X}(0)$ is an arbitrary but fixed point on Γ.

To look at a nontrivial example, suppose there are three intersections in a stencil; for notation refer to Figure 1. We show how to correct discretizations of Δu and $u_{xy} = u_{yx}$ at the boldface gridpoint (x_i, y_j) in Figure 1. Apply Lemma 4 (a) in the y-direction and Lemma 3 in the x-direction and get

$$\begin{aligned}\Delta u(x_i, y_j) \approx{}& \frac{u(x_{i+1}, y_j) + u(x_{i-1}, y_j) + u(x_i, y_{j+1}) + u(x_i, y_{j-1}) - 4u(x_i, y_j)}{h^2} \\ &- \frac{1}{h^2}\sum_{m=0}^{3} \frac{(k_2^+)^m}{m!}\left[\frac{\partial^m u}{\partial y^m}\right]_{\alpha_2} - \frac{1}{h^2}\sum_{m=0}^{3} \frac{(k_4^+)^m}{m!}\left[\frac{\partial^m u}{\partial y^m}\right]_{\alpha_4} \\ &- \frac{1}{h^2}\sum_{m=0}^{3} \frac{(h_3^+)^m}{m!}\left[\frac{\partial^m u}{\partial x^m}\right]_{\alpha_3} + O\big(h^2\big)\,,\end{aligned} \tag{27}$$

where we assume a uniform mesh with $\Delta x = \Delta y = h$. The $k^\pm$ variables indicate signed distances in the y-direction and the $h^\pm$ variables indicate signed distances in

[5] This is true also for varying ρ, as long as $(\rho-1)u_{xxx}^-$ is bounded.

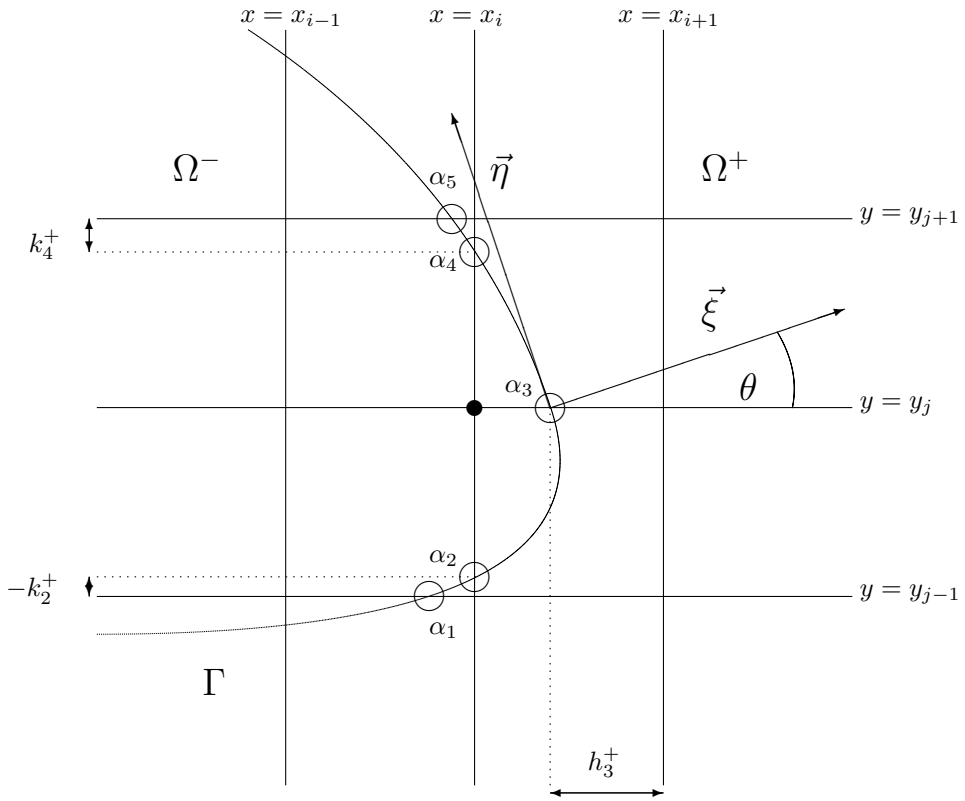

FIG. 1. *Interface and mesh geometry near a lattice point (x_i, y_j). We show the oriented tangent ($\vec{\eta}$) and normal ($\vec{\xi}$) directions to the interface at a selected intersection with a horizontal mesh line, and the angle (θ) that the outward normal forms with the positive horizontal direction. Five intersections of the interface and the mesh are of interest here; they are labeled $\alpha_1, \alpha_2, \ldots, \alpha_5$.*

the x-direction. The "+" variables are found by subtracting coordinates of α from coordinates of grid points in Ω^+ and the "−" variables are found by subtracting coordinates of α from coordinates of grid points in Ω^-. This generalization of the 1D case is convenient because later we develop one-sided Taylor expansions about α. In two or higher dimensions, it is convenient to define

$$\lim_{x \to \alpha^+} \text{ to mean } \lim_{x \in \Omega^+, x \to \alpha}.$$

The "−" on the first correction term in (27) does not agree with the sign in (8) because this definition reverses the sign of the jump at α_2 compared to 1D. This choice is made so that the formulas do not depend on points in Ω^+ having larger coordinates than points in Ω^-, always yielding a $-$ in front of corrections on the $+$ side, and a $+$ sign on corrections on the $-$ side. If we reverse the roles of Ω^- and Ω^+, the jumps but also the $1/h^2$ factor change sign, while h^- and h^+ are simply switched. To illustrate this point, we also show the corrections for the point (x_i, y_{j-1}):

$$\begin{aligned}\Delta u(x_i, y_j) \approx{}& \frac{u(x_{i+1}, y_{j-1}) + u(x_{i-1}, y_{j-1}) + u(x_i, y_j) + u(x_i, y_{j-2}) - 4u(x_i, y_{j-1})}{h^2} \\ &+ \frac{1}{h^2} \sum_{m=0}^{3} \frac{(h_1^-)^m}{m!} \left[\frac{\partial^m u}{\partial x^m}\right]_{\alpha_1} + \frac{1}{h^2} \sum_{m=0}^{3} \frac{(k_2^-)^m}{m!} \left[\frac{\partial^m u}{\partial y^m}\right]_{\alpha_2} + O(h^2); \end{aligned} \tag{28}$$

please compare the terms involving $[.]_{\alpha_2}$ in (27) and (28).

Cross derivatives are a little more tricky. Suppose we wish to correct the approximation

$$u_{xy}(x_i, y_j) \approx \frac{\{u(x_{i+1}, y_{j+1}) - u(x_{i-1}, y_{j+1})\} - \{u(x_{i+1}, y_{j-1}) - u(x_{i-1}, y_{j-1})\}}{4h^2},$$

which for smooth u is identical to

$$u_{yx}(x_i, y_j) \approx \frac{\{u(x_{i+1}, y_{j+1}) - u(x_{i+1}, y_{j-1})\} - \{u(x_{i-1}, y_{j+1}) - u(x_{i-1}, y_{j-1})\}}{4h^2}.$$

With notation as in Figure 1 we see that these two expressions give rise to distinct corrected versions, but with truncation error of the same order. If we do differences in y first, then

$$u_y(x_{i+1}, y_j) \approx \frac{u(x_{i+1}, y_{j+1}) - u(x_{i+1}, y_{j-1})}{2h},$$
$$u_y(x_{i-1}, y_j) \approx \frac{u(x_{i-1}, y_{j+1}) - u(x_{i-1}, y_{j-1})}{2h}.$$

Based on these and using Lemma 3 for u_y,

$$u_{yx}(x_i, y_j) \approx \frac{\{u(x_{i+1}, y_{j+1}) - u(x_{i-1}, y_{j+1})\} - \{u(x_{i+1}, y_{j-1}) - u(x_{i-1}, y_{j-1})\}}{4h^2} - \frac{1}{2h} \sum_{m=0}^{2} \frac{(h_3^+)^m}{m!} \left[\frac{\partial^{m+1} u}{\partial y \partial x^m}\right]_{\alpha_3}.$$

If we compute differences in x first, the approximations for $u_x(x_i, y_{j+1})$ and $u_x(x_i, y_{j-1})$ have to be corrected via Lemma 3 at α_1 and α_5, respectively, and the differences for $u_{xy}(x_i, y_j)$ need to be corrected according to Lemma 4 at α_2 and α_4.

REMARK 23. *In cases where the equality of u_{xy} and u_{yx} is also desired for the approximations, one may wish to take the average of the two corrected forms.*

It should be clear how general finite differences of arbitrary order can be corrected with this approach, provided one knows the intersections of the interface with the mesh and the jumps there. We call the application of the corrections described in this section EJIIM. It differs from IIM [4] by

- correcting standard differences instead of finding completely new differences (γs, see [4]);
- being independent of the particular jump conditions;
- separating the contributions from the jumps in u and its derivatives;
- using jumps in the Cartesian coordinate directions, including introducing multiple corrections for a mesh point;
- allowing the use of third and even higher order correction terms.

4. Jumps for selected problems. The first question from the introduction is more difficult to answer. The jumps depend on the PDE, or actually the problem that the PDE models. For simplicity and explicitness, we consider elliptic equations in 2D with three types of jump conditions. Below, Ω is the rectangular computational domain.

Recall that $\Gamma = \vec{X}(t) = (x(t), y(t))$ is parameterized by arclength t. The normalized tangent direction to Γ at t is $\vec{\eta}(t) = (\dot{x}(t), \dot{y}(t)) = (-\sin(\theta(t)), \cos(\theta(t)))$, where

$\theta(t)$ is the angle from the vector $(1,0)$ to the outward normal $\vec{\xi}(t) = (\cos\theta(t), \sin\theta(t))$ to Γ at t. See Figure 1. The formulas are this simple because we parameterize by arclength.

(a) *Poisson problems with known singular sources.* f is smooth at least in $\Omega \setminus \Gamma$,

$$\Delta u(x) = f(x) + \int_\Gamma v(t)\delta\left(x - \vec{X}(t)\right) + w(t)\delta'\left((x - \vec{X}(t)) \cdot \vec{\xi}(t)\right) dt, \tag{29}$$

$$u = 0 \text{ on } \partial\Omega. \tag{30}$$

Later, in section 7.1, we will see an instance of this problem where f and w vanish and v is constant. The solution to (29) satisfies $[u] = w$ and $[u_\xi] = v$.

(b) *BVP on irregular domains.* $\Omega^- \subset \Omega$ is a connected domain with smooth boundary $\Gamma = \partial\Omega^-$,

$$\Delta u = f(x,y) \text{ in } \Omega^-, \tag{31}$$

$$u = \bar{u} \text{ on } \partial\Omega^-. \tag{32}$$

Later, in section 7.2, we will see instances of this problem, for the cases where $\partial\Omega^- \cap \partial\Omega$ is empty and nonempty, for both "interior" and "exterior" BVPs.

(c) *Composite material problems.* f and β may be discontinuous across an interface Γ and

$$\nabla \cdot (\beta \nabla u) = f(x,y) \text{ in } \Omega, \tag{33}$$

$$u = \bar{u} \text{ on } \partial\Omega. \tag{34}$$

Later, in sections 7.3 and 7.4, we will see instances of this problem, with piecewise constant and piecewise smooth but not piecewise constant coefficients.

Considering only these cases is just for brevity of exposition. The use of EJIIM is by no means restricted to these simple cases. Section 7.5 shows instances of the more general problem (again $\Omega^- \subset \Omega$)

$$\nabla \cdot (\beta \nabla u) + \kappa u = f(x,y) \text{ in } \Omega^-, \tag{35}$$

$$lu + (1-l)u_\xi = \gamma \text{ on } \partial\Omega^-, \tag{36}$$

with multiply connected Ω^- and various boundary conditions on several interfaces, which demonstrate the real strength of EJIIM.

4.1. Problem (a). Problem (a) is the easiest to solve after the jumps are derived, because they are independent of u. The jumps in the function and normal derivative across the interface, together with the equation, determine all other jumps

(via tangential derivatives on the lower order equations) as follows:

$$
\begin{aligned}
[u] &= w,\\
[u_\eta] &= w',\\
[u_\xi] &= v,\\
[u_{\eta\eta}] &= w'' + \theta' v,\\
[u_{\xi\eta}] &= v' - \theta' w',\\
[u_{\xi\xi}] &= [f] - w'' - \theta' v,\\
[u_{\eta\eta\eta}] &= w''' + 3\theta' v' - 2\left(\theta'\right)^2 w' + \theta'' v,\\
[u_{\xi\eta\eta}] &= v'' - 3\theta' w'' - 2\left(\theta'\right)^2 v + [f]\theta' - \theta'' w',\\
[u_{\xi\xi\eta}] &= [f]' - w''' - 3\theta' v' + 2\left(\theta'\right)^2 w' - \theta'' v,\\
[u_{\xi\xi\xi}] &= [f_\xi] - v'' + 3\theta' w'' + 2\left(\theta'\right)^2 v - [f]\theta' + \theta'' w'.
\end{aligned}
\tag{37}
$$

For a detailed derivation of these jumps, see [4, 16]. Note that the directions in which the derivatives are taken depend on t. Here and from now on, we suppress the dependence on t in our notation, but equations involving jumps ($[.]$) hold for all t, and the directions of normal and tangential derivatives depend on t.

4.2. Problem (b). Problem (b) is one of domain imbedding, which is usually done to take advantage of fast solvers on the larger, regular domain. The key idea of our approach, which is different from Yang's IIM for boundary value problems [18], Mayo's approach [8], and also Proskurowski and Widlund's approach [11], is to extend f and the solution u to be identically zero in the complement Ω^+ of Ω^-. Of course, this is only possible by allowing both $[u] \neq 0$ and $[u_\xi] \neq 0$, effectively making an ansatz of a sum of both a double and a single layer potential. This ansatz introduces more variables but makes for very simple jump conditions, which immediately yield the values for some of these variables:

$$
\begin{aligned}
[u] &= -\bar{u},\\
[u_x] &= -u_x^-,\\
[u_y] &= -u_y^-,\\
[u_{xx}] &= -u_{xx}^-,\\
[u_{yy}] &= -u_{yy}^-.
\end{aligned}
\tag{38}
$$

For components of Ω^+ that share a boundary with $\partial\Omega$, this amounts to a mixed BVP (Dirichlet zero on $\partial\Omega$, Neumann zero on the boundary shared with Ω^-) which has exactly the trivial solution, so our ansatz of extension by zero is justified. On components of Ω^+ whose boundaries do not partially coincide with $\partial\Omega$, we get a Neumann problem which has constants as solutions. Imposing that the numerical solution be zero on the grid points in Ω^+ along the interface on these components creates a "corridor" with Neumann zero and Dirichlet zero boundary conditions along the interface and a Dirichlet problem with zero boundary conditions in the interior of these components of Ω^+. The solution to these is clearly zero.

We can eliminate the limits of second and higher derivatives from the jump equa-

tions, by writing

$$[\Delta u] = f^-,$$
$$\left[\frac{\partial^n(\Delta u)}{\partial \xi^n}\right] = \left[\frac{\partial^n f^-}{\partial \xi^n}\right],$$

and then using the formulas for Problem (a), observing that $v = -u_\xi^-$ and replacing derivatives of w using $w' = -\bar{u}'$, $w'' = -\bar{u}''$, etc. This idea comes from [6], where splines are used to approximate the derivatives along the interface. It halves the number of auxiliary variables and should have significant impact in computations, but has not been explored further yet.

For a Neumann boundary condition $u_\xi = \hat{u}$ replacing (34) on an interior boundary, the jumps are derived from the same ansatz (extension by zero), but now with $[u_\xi] = -\hat{u}$; we obtain

$$\begin{aligned}
[u] &= -u^-,\\
[u_x] &= -\cos\theta\hat{u} - \sin\theta u_\eta^-,\\
[u_y] &= -\sin\theta\hat{u} + \cos\theta u_\eta^-,\\
[u_{xx}] &= -u_{xx}^-,\\
[u_{yy}] &= -u_{yy}^-.
\end{aligned}$$

The distinction between components as in the Dirichlet problem case does not exist in this case. The limit u^+ on $\partial\Omega^+$ is zero, and the Dirichlet problem on these components has exactly the trivial solution.

4.3. Problem (c). Problem (c) is the hardest to solve numerically and was the motivation for our initial interest. When trying to find the location of interfaces between different constant values for β (an inverse problem) with IIM [4], we found that the method was not stable enough for large contrast ($\rho = \beta^-/\beta^+ \gg 1$) problems. EJIIM was developed after many ideas from [1, 6, 8] and others to overcome this problem. Later we realized the much broader applicability of this approach. We assume that the jump conditions are

$$\begin{aligned}
[u] &= w(t),\\
[\beta u_\xi] &= \tilde{v}(t),
\end{aligned}$$

where the physical conditions are usually $w = \tilde{v} = 0$. Equation (33) provides at least two ways to derive another jump condition. By taking limits on both sides of the interface we get

$$\beta^+\left(u_{\xi\xi}^+ + u_{\eta\eta}^+\right) + \nabla\beta^+ \cdot \nabla u^+ = f^+, \tag{39}$$

$$\beta^-\left(u_{\xi\xi}^- + u_{\eta\eta}^-\right) + \nabla\beta^- \cdot \nabla u^- = f^-. \tag{40}$$

Extending Li's ideas in [6] to piecewise smooth (but not piecewise constant) coefficients, we can divide by β and then discretize the divided equation

$$\Delta u + \frac{\nabla\beta \cdot \nabla u}{\beta} = \frac{f}{\beta}, \tag{41}$$

which holds everywhere except at points on Γ. The jumps at Γ are (see [4, 5, 16])

$$
\begin{aligned}
[u] &= w, \\
[u_\eta] &= w', \\
[u_\xi] &= \frac{\tilde{v}}{\beta^+} + (\rho - 1)u_\xi^-, \\
[u_{\eta\eta}] &= w'' + \theta'[u_\xi], \\
[u_{\xi\eta}] &= \frac{\beta_\eta^- \beta^+ - \beta^- \beta_\eta^+}{(\beta^+)^2} u_\xi^- + (\rho - 1)\left(u_{\xi\eta}^- + \theta' u_\eta^-\right) - \theta'[u_\eta], \\
[u_{\xi\xi}] &= (\rho - 1)\left(u_{\xi\eta}^- + u_{\eta\eta}^-\right) - [u_{\eta\eta}] \\
&\quad + \frac{1}{\beta^+}\left([f] + \beta_\xi^- u_\xi^- + \beta_\eta^- u_\eta^- - \beta_\xi^+\left(u_\xi^- + [u_\xi]\right) - \beta_\eta^+\left(u_\eta^- + [u_\eta]\right)\right).
\end{aligned}
\tag{42}
$$

$[u_\eta]$, $[u_{\eta\eta}]$, and $[u_{\xi\eta}]$ are found by differentiating lower order jumps, while $[u_{\xi\xi}]$ comes from dividing both (39) and (40) by β^+. In section 7.3, this approach is used in the simpler case of constant coefficients.

Translating Li's technique in [6] into our notation, one may also derive two different jump conditions. Writing for short

$$v = \frac{\tilde{v}}{\beta^+} + (\rho - 1)u_\xi^-,$$

Li [6] approximates v' by fitting a spline and then taking its derivative. Dividing (40) by β^- instead of β^+ provides more equations for second order jumps:

$$
\begin{aligned}
\left[\Delta u + \frac{\nabla\beta \cdot \nabla u}{\beta}\right] &= \left[\frac{f}{\beta}\right], \\
[u_{\xi\eta}] &= v' - \theta'[u_\eta], \\
[u_{\xi\xi}] &= \left[\frac{f}{\beta}\right] - [u_{\eta\eta}] - \left[\frac{\beta_\xi u_\xi}{\beta}\right] - \left[\frac{\beta_\eta u_\eta}{\beta}\right].
\end{aligned}
$$

After eliminating $[u_{\eta\eta}]$, the last two equations have the advantage of not using one-sided limits of second derivatives. We do not currently use these later forms of the jumps in computations, but point out that [6] does and that we wish to experiment with them in the future.

REMARK 24. *For Problem* (a)*, we include the third order jump corrections because this allows an easy second order convergence proof; see Theorem* 26*. However, in numerical experiments it is observed that in all cases* (a), (b)*, and* (c)*, it suffices to have a truncation error that is* $O(h)$ *near the interface and* $O(h^2)$ *elsewhere to get* $O(h^2)$ *errors in the solution in the max norm* (*second order convergence*).

4.4. Problem (c) via Liouville transformation. We also explore a different approach to Problem (c) with variable coefficients, known for smooth coefficients as the Liouville transformation (Stefanesco transformation). We change variables:

$\tilde{u} = \sqrt{\beta}u$. Then

$$\begin{aligned}\Delta\tilde{u} &= \Delta\left(\sqrt{\beta}\right)u + 2\nabla\left(\sqrt{\beta}\right)\cdot\nabla u + \sqrt{\beta}\Delta u \\ &= \frac{\Delta\left(\sqrt{\beta}\right)}{\sqrt{\beta}}\tilde{u} + \sqrt{\beta}\left(\frac{\nabla\beta\cdot\nabla u}{\beta} + \Delta u\right) \\ &\overset{\text{using (41)}}{=} \frac{\Delta\left(\sqrt{\beta}\right)}{\sqrt{\beta}}\tilde{u} + \frac{f}{\sqrt{\beta}},\end{aligned}$$

and finally

$$\Delta\tilde{u} - \frac{\Delta\left(\sqrt{\beta}\right)}{\sqrt{\beta}}\tilde{u} = \frac{f}{\sqrt{\beta}}. \tag{43}$$

This turns the problem into a variable coefficient Helmholtz equation, of the form of (35). Of course, this equation is only valid away from the interface. To use EJIIM, we also need to derive the jump conditions for $\tilde{u}$; for details see [16]. For example, the solution $\tilde{u}$ inherits the discontinuity from β.

(44)

$$\begin{aligned}[\tilde{u}] &= \left(\rho^{-1/2} - 1\right)\tilde{u}^-, \\ [\tilde{u}_\xi] &= \left(\rho^{1/2} - 1\right)\tilde{u}^-_\xi + \frac{\beta^+_\xi}{\beta^+}[\tilde{u}] + \frac{[(\sqrt{\beta})_\xi]\tilde{u}^-}{\sqrt{\beta^+}}, \\ [\Delta\tilde{u}] &= \left[\frac{f}{\sqrt{\beta}}\right] + \left[\frac{\Delta(\sqrt{\beta})}{\sqrt{\beta}}\right]\tilde{u}^- + \frac{\Delta(\sqrt{\beta})^+}{\sqrt{\beta^+}}[\tilde{u}], \\ [\tilde{u}_\eta] &= -\frac{\rho^{-3/2}\rho_\eta}{2}\tilde{u}^- + \left(\rho^{-1/2} - 1\right)\tilde{u}^-_\eta, \\ [\tilde{u}_{\eta\eta}] &= \theta'[\tilde{u}_\xi] - \rho^{-3/2}\rho_\eta\tilde{u}^-_\eta + \frac{3\rho^{-5/2}\rho_\eta^2 - 2\rho^{-3/2}\left(-\theta'\rho_\xi + \rho_{\eta\eta}\right)}{4}\tilde{u}^- \\ &\quad + \left(\rho^{-1/2} - 1\right)\left(-\theta'\tilde{u}^-_\xi + \tilde{u}^-_{\eta\eta}\right), \\ [\tilde{u}_{\xi\eta}] &= -\theta'[\tilde{u}_\eta] + \frac{\rho^{-1/2}\rho_\eta}{2}\tilde{u}^-_\xi + \left(\rho^{1/2} - 1\right)\left(\tilde{u}^-_{\eta\xi} + \theta'\tilde{u}^-_\eta\right) \\ &\quad + \frac{\left(\beta^+_{\eta\xi} + \theta'\beta^+_\eta\right)\beta^+ - \beta^+_\eta\beta^+_\xi}{\left(\beta^+\right)^2}[\tilde{u}] + \frac{\beta^+_\xi}{\beta^+}[\tilde{u}_\eta] - \left[\frac{\beta_\xi}{2\sqrt{\beta}}\right]\beta^+_\eta\frac{\left(\beta^+\right)^{-3/2}}{2}\tilde{u}^- \\ &\quad + \left[2\left(\beta_{\xi\eta} + \theta'\beta_\eta\right)\beta^{-1/2} - \beta_\xi\beta_\eta\beta^{-3/2}\right]\frac{\left(\beta^+\right)^{-1/2}}{4}\tilde{u}^- + \left[\frac{\beta_\xi}{2\sqrt{\beta}}\right]\left(\beta^+\right)^{-1/2}\tilde{u}^-_\eta.\end{aligned}$$

The fourth and fifth jump equation are derived by taking derivatives of the first equation, and the sixth equation is derived from the second equation. The validity of these conditions is (partially) numerically verified in section 7.4 (many terms vanish in that example because of the special choice of β.)

5. Jumps in local and Cartesian coordinates. Formulas for the jumps were derived in section 4.2 in the coordinate directions or in sections 4.1, 4.3, and 4.4 in

the normal and tangential directions, in the following form:

$$\begin{aligned}
[u](t) &= w(t, u^-(t)),\\
[u_\xi](t) &= w_1(t, u^-, u_\xi^-, u_\eta^-),\\
[u_\eta](t) &= w_2(t, u^-, u_\xi^-, u_\eta^-),\\
[u_{\xi\xi}](t) &= w_{11}(t, u^-, u_\xi^-, u_\eta^-, u_{\xi\xi}^-, u_{\xi\eta}^-, u_{\eta\eta}^-),\\
[u_{\xi\eta}](t) &= w_{12}(t, u^-, \dots),\\
[u_{\eta\eta}](t) &= w_{22}(t, u^-, \dots),\\
[u_{\xi\xi\xi}](t) &= w_{111}(t, u^-, \dots),\\
[u_{\xi\xi\eta}](t) &= w_{112}(t, u^-, \dots),\\
[u_{\xi\eta\eta}](t) &= w_{122}(t, u^-, \dots),\\
[u_{\eta\eta\eta}](t) &= w_{222}(t, u^-, \dots).
\end{aligned}$$

We assume it is always possible to write the jumps in a form that uses only limits on u and its derivatives from one fixed side of the interface, which is the case at least for the elliptic problems that we consider here.

To use Lemma 3 or Lemma 4, we change coordinates for the jumps. For a fixed intersection $(x(t_\circ), y(t_\circ))$ of Γ with the mesh we introduce local coordinates as follows. The origin is placed at $(x(t_\circ), y(t_\circ))$, and the local coordinate axes are parallel to the tangent and normal to Γ at $(x(t_\circ), y(t_\circ))$. In these coordinates, the interface is expressed as a function of arclength by

$$\begin{pmatrix}\xi(t)\\ \eta(t)\end{pmatrix} = \begin{pmatrix}\cos\theta(t_\circ) & \sin\theta(t_\circ)\\ -\sin\theta(t_\circ) & \cos\theta(t_\circ)\end{pmatrix}\begin{pmatrix}x(t)-x(t_\circ)\\ y(t)-y(t_\circ)\end{pmatrix}.$$

Writing for short $c = \cos\theta(t_\circ)$ and $s = \sin\theta(t_\circ)$, one finds the following jumps at $(x(t_\circ), y(t_\circ))$:

$$\begin{pmatrix}[u_x]\\ [u_y]\end{pmatrix} = \begin{pmatrix}c & -s\\ s & c\end{pmatrix}\begin{pmatrix}[u_\xi]\\ [u_\eta]\end{pmatrix},$$

$$\begin{pmatrix}[u_{xx}]\\ [u_{xy}]\\ [u_{yy}]\end{pmatrix} = \begin{pmatrix}c^2 & -2cs & s^2\\ cs & c^2-s^2 & -cs\\ s^2 & 2cs & c^2\end{pmatrix}\begin{pmatrix}[u_{\xi\xi}]\\ [u_{\xi\eta}]\\ [u_{\eta\eta}]\end{pmatrix},$$

$$\begin{pmatrix}[u_{xxx}]\\ [u_{xxy}]\\ [u_{xyy}]\\ [u_{yyy}]\end{pmatrix} = \begin{pmatrix}c^3 & -3c^2s & 3cs^2 & -s^3\\ c^2s & c^3-2cs^2 & s^3-2c^2s & cs^2\\ cs^2 & 2c^2s-s^3 & c^3-2cs^2 & -c^2s\\ s^3 & 3s^2c & 3c^2s & c^3\end{pmatrix}\begin{pmatrix}[u_{\xi\xi\xi}]\\ [u_{\xi\xi\eta}]\\ [u_{\xi\eta\eta}]\\ [u_{\eta\eta\eta}]\end{pmatrix};$$

there are similar formulas (simply replace s by $-s$) for the inverse transformations. To derive, for instance, w_{12} from w_1, one needs some quantities about the interface. All those can be derived from the general formulas

$$\begin{aligned}
\frac{d^n\xi}{dt^n}(t_\circ) &= c\frac{d^nx}{dt^n}(t_\circ) + s\frac{d^ny}{dt^n}(t_\circ),\\
\frac{d^n\eta}{dt^n}(t_\circ) &= -s\frac{d^nx}{dt^n}(t_\circ) + c\frac{d^ny}{dt^n}(t_\circ).
\end{aligned}$$

6. The difference schemes.

6.1. Convergence proof for singular sources. First consider the case of singular sources, Problem (a), where all jumps are known. The Poisson problem on the rectangle $\Omega = (0, n_x h) \times (0, n_y h) = (0, a) \times (0, b)$ with smooth right-hand side is discretized on the grid $(x_i, y_j) = (ih, jh)$ via the standard 5-point stencil, (2), as

$$\Delta_h U = F.$$

Here and from now on, the vector $U \in \mathbf{R}^{(n_x-1)\times(n_y-1)}$ denotes the numerical approximation to u at the grid points in the interior of Ω in the "natural order," i.e., the grid function that satisfies our discretization of the partial differential equation under consideration. F is the vector of values of f at these points.

We order the intersections of Γ with the mesh with increasing arclength t. If an intersection of Γ with the mesh agrees with a gridpoint, it may have to be treated as one, two, or three intersections. For example, if we shift the interface in Figure 1 to the left, so that α_3 agrees with (x_i, y_j), then we have two possibilities, depending on whether we want the approximation to $u(x_i, y_j)$ to approximate the limit in Ω^- or the limit in Ω^+. In the former case, the intersection with the horizontal line $y = y_j$ belongs in the interval $[x_i, x_{i+1}]$ and the intersection with the vertical line $x = x_i$ belongs in the interval $[y_j, y_{j+1}]$. In the latter case, the intervals are $[x_{i-1}, x_i]$ and $[y_{j-1}, y_j]$, respectively. If the tangent to the interface at the gridpoint is parallel to one of the coordinate axes, the two cases to be distinguished involve one or three intersections.

The vector $C \in \mathbf{R}^{4m}$ of approximations of the jumps in u has four entries for each of the m intersections, counting multiplicities as described in the previous paragraph. Depending on the type of intersection (with a horizontal or vertical mesh line), the elements of C approximate jumps in derivatives in the x- or y-direction. Given the first few intersections as in Figure 1,

$$C = [[u]_{\alpha_1}, [u_x]_{\alpha_1}, [u_{xx}]_{\alpha_1}, [u_{xxx}]_{\alpha_1}, [u]_{\alpha_2}, [u_y]_{\alpha_2}, [u_{yy}]_{\alpha_2}, [u_{yyy}]_{\alpha_2}, [u]_{\alpha_3}, [u_x]_{\alpha_3}, \dots]^T.$$

Each jump is used twice to correct the standard differences, namely for the two grid points neighboring the intersection. For example, jumps at α_3 are used to correct differences (approximating x-derivatives) at (x_i, y_j) and (x_{i+1}, y_j). The coefficients for the jump in the mth derivative are $-(h_3^+)^m/(m!h^2)$ and $(h_3^-)^m/(m!h^2)$, respectively.

We write all these coefficients into the matrix Ψ, where rows are ordered like the grid points, and columns are ordered like the jumps. The two nonzero entries per column correspond to the two grid points where the differences are being corrected. Hence, equations like (27) say how to correct the right-hand side of the equation for (x_i, y_j). We combine all the needed corrections into the system

$$\Delta_h U = F + \Psi C. \tag{45}$$

REMARK 25. *If we correct only to second order, then $C \in \mathbf{R}^{3m}$. Also, it is convenient to eliminate known jumps and absorb them into F to further shorten C.*

The discrete system (45) mimics the PDE (29) in that we have correction terms only on the right-hand side of the system, but the differential operator (difference operator) is the usual one. This feature is similar to Peskin's Immersed Boundary Method [10], a first order predecessor of the IIM. Peskin's view of a discrete delta function on the right-hand side of (45) is further explored in the context of EJIIM in 1D in the first author's thesis, [16].

Eu denotes the restriction of u to the grid. Our discretization has $O(h^2)$ truncation error, i.e.,

$$\Delta_h Eu = F + \Psi C + O(h^2).$$

Since the truncation error is $O(h^2)$ for all equations, the standard convergence proof (based on a discrete maximum principle, see, for example, section 6.2 in Morton and Mayers [9]) for the Poisson problem on rectangles carries over to this case.

THEOREM 26 (second order convergence). *For a Poisson problem with singular sources, numerical solutions obtained by discretization with EJIIM including up to third order jumps satisfy*

$$\|\Delta_h^{-1}(F + \Psi C) - Eu\|_\infty = O(h^2).$$

Proof. Let the error in the solution be $T = U - Eu$, and denote the bound on the truncation error $\Delta_h T = F + \Psi C - \Delta_h Eu$ on the rectangle $(0, n_x h) \times (0, n_y h) = (0, a) \times (0, b)$ by $\|\Delta_h T\|_\infty \le Kh^2$ for $h < h_\circ$.

Now extend $\Delta_h \in \mathbf{R}^{(n_x-1)(n_y-1)\times(n_x-1)(n_y-1)}$ to $\tilde{\Delta}_h \in \mathbf{R}^{(n_x-1)(n_y-1)\times(n_x+1)(n_y+1)}$ by including the boundary contributions, i.e., using the standard approximation (2) for all interior points. Extending U by the values of $\tilde{E}u$ on the boundary (all zero) in the appropriate order, we see that $\tilde{\Delta}_h \tilde{U} = \Delta_h U$. Similarly, extend $\tilde{T}$ (by zero, since the boundary values are exact) and see that $\|\tilde{\Delta}_h \tilde{T}\|_\infty \le Kh^2$.

Define the entries of the vector Φ by $\Phi_{ij} = (x_i - a/2)^2 + (y_j - b/2)^2$ for $i = 0, 1, \ldots, n_x$ and $j = 0, 1, \ldots n_y$; then $\tilde{\Delta}_h \Phi = [4, 4, \ldots, 4]^T$. Let $\Xi = \tilde{T} + Kh^2\Phi/4$, then $(\tilde{\Delta}_h \Xi)_{ij} \ge 0$. $\tilde{\Delta}_h$ satisfies a discrete maximum principle, i.e., $u_{i,j+1} + u_{i,j-1} + u_{i+1,j} + u_{i-1,j} - 4u_{i,j} \ge 0$ implies $u_{i,j} \le \max(u_{i,j+1}, u_{i,j-1}, u_{i+1,j}, u_{i-1,j})$, so Ξ assumes its maximum at a boundary point. But $\tilde{T}$ vanishes on the boundary, and Φ has its maximum at the corners, so

$$\tilde{T}_{i,j} \le \Xi_{i,j} \le \frac{a^2 + b^2}{16} Kh^2.$$

Repeating the argument with $\Xi = Kh^2\Phi/4 - \tilde{T}$, we arrive at

$$\|T\|_\infty = \|\tilde{T}\|_\infty \le \frac{a^2 + b^2}{16} Kh^2. \qquad \square$$

REMARK 27. *The special case where no singular source is present and f is simply discontinuous across the interface is also covered by our corrections, and consequently by Theorem* 26.

6.2. Discretization of solution-dependent jumps. For the other two problems, (b) and (c), some of the jumps depend on the solution, which in turn depends on the boundary conditions and coefficients. Suppose we knew the solution on the grid, just as we made the ansatz of knowing the jumps before. Then we could get approximations to the quantities on the right-hand side of the jump equations (37), (38), (42), or (44) by fitting a low degree polynomial $p(x, y)$ through six points (for $O(h)$ truncation error near the interface) or ten points (for $O(h^2)$ truncation error), which have to lie on the same side of the interface. In Problem (b) that means the points lie in Ω^-, while in Problem (c) we have a choice of either side. For the sake of explicitness, we will write one-sided limits with superscript "$-$" to indicate the limiting operation in the chosen region, after possibly renaming the regions in Problem (c).

The value of p on the interface is an approximation for u, and derivatives of p approximate derivatives of u with decreasing accuracy for higher derivatives. The points have to be such that uniform bounds are possible for these approximations. The following lemmas provide such bounds.

Given six points $P_0(h_0, k_0)$, $P_1(h_1, k_1)$, $P_2(h_2, k_2)$, $P_3(h_3, k_3)$, $P_4(h_4, k_4)$, and $P_5(h_5, k_5)$, define the Vandermonde matrix of bivariate Lagrange interpolation by quadratic polynomials in two variables on these six nodes

$$\mathcal{P} = \begin{bmatrix} 1 & h_0 & k_0 & h_0^2 & h_0k_0 & k_0^2 \\ 1 & h_1 & k_1 & h_1^2 & h_1k_1 & k_1^2 \\ 1 & h_2 & k_2 & h_2^2 & h_2k_2 & k_2^2 \\ 1 & h_3 & k_3 & h_3^2 & h_3k_3 & k_3^2 \\ 1 & h_4 & k_4 & h_4^2 & h_4k_4 & k_4^2 \\ 1 & h_5 & k_5 & h_5^2 & h_5k_5 & k_5^2 \end{bmatrix}, \tag{46}$$

and the quantities $l_{ijm} = (h_i - h_j)(k_m - k_j) - (k_i - k_j)(h_m - h_j)$, for $i, j, m \in \{0, 1, 2, 3, 4, 5\}$.

LEMMA 28. *Interpolation of u by polynomials $p(x, y) = p_0 + p_1x + p_2y + p_3x^2 + p_4xy + p_5y^2$ on the points P_0, P_1, P_2, P_3, P_4, and P_5 is always possible if and only if* $\det \mathcal{P} \neq 0$.

Proof. Let the vector of values of u at the six points be denoted by $F = [f_0, f_1, f_2, f_3, f_4, f_5]^T$ and define $P = [p_0, p_1, p_2, p_3, p_4, p_5]^T$. The fact that $p(x, y)$ satisfies $p(h_i, k_i) = f_i$ for $i \in \{0, 1, 2, 3, 4, 5\}$ can be written as $\mathcal{P}P = F$, which has a solution for arbitrary F if and only if $\det \mathcal{P} \neq 0$. ∎

LEMMA 29 (see Lorentz [7, Theorem 11.2.1]).

$$\det \mathcal{P} = l_{015}l_{325}l_{034}l_{124} - l_{014}l_{324}l_{035}l_{125}.$$

COROLLARY 30. *If P_0, P_1, and P_5 are on a line, none of P_2, P_3, and P_4 is on that line, and P_2, P_3, and P_4 are not on any line, then interpolation by quadratic polynomials is possible on these points.*

Proof. Noting that l_{ijm} is twice the signed area of the triangle formed by the nodes P_i, P_j, P_m, if P_0, P_1, and P_5 are on a line, then $l_{015}l_{325}l_{034}l_{124} = 0$ since $l_{015} = 0$. By hypothesis, none of the other triangles is degenerate. This means that all of l_{014}, l_{035}, l_{125}, and l_{324} are nonzero. So $\det \mathcal{P} = -l_{014}l_{324}l_{035}l_{125} \neq 0$. ∎

REMARK 31. *Lorentz* [7] *also provides a reference to a similar result needed for the extension of EJIIM to 3D.*

Given $\mathcal{I}$, the set of intersections of the interface with the mesh lines, our algorithm is designed to find six points in Ω^- satisfying the hypothesis in Corollary 30, by making the closest grid point in Ω^- the "anchor" point and selecting five more "neighbors" on the grid, as shown in Figure 2.

LEMMA 32 (curve condition). *If for every intersection in $\mathcal{I}$, one of the two disks of radius $\sqrt{5/2}\,h$ and tangent to Γ at $\mathcal{I}$ lies entirely in Ω^-, then it is possible to find six grid points in Ω^- as required in Corollary* 30.

Proof. It suffices to show that any closed disk of radius $\sqrt{5/2}\,h$ contains six grid points in the position required by Corollary 30. By rotating the mesh by $\pi/2$, π, or $3\pi/2$, and shifting by multiples of $h/2$, we may assume that the mesh is of the form $x_i = ih + h/2$ and $y_j = jh + j/2$ for $i, j \in \mathbf{Z}$, and that the center of the disk in the hypothesis lies in $[0, h/2] \times [0, h/2]$. The six points $(-h/2, -h/2)$, $(-h/2, h/2)$, $(h/2, -h/2)$, $(h/2, h/2)$, $(h/2, 3h/2)$, $(3h/2, h/2)$ are in the position as required and all lie in the disk. This is easily seen by observing that the disks of radius $\sqrt{5/2}\,h$

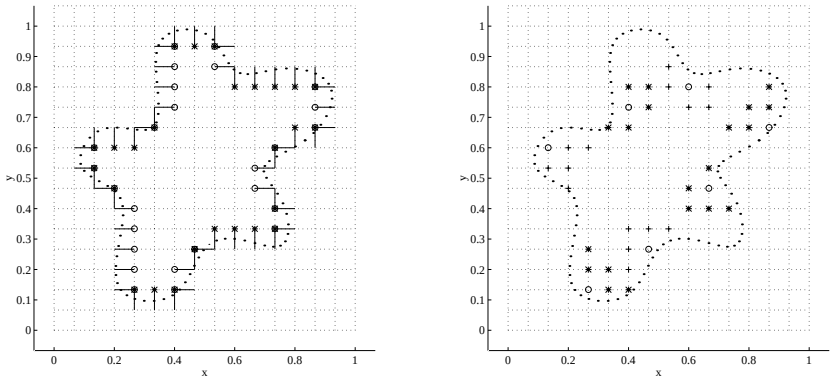

FIG. 2. *In* (a)*, we see all the anchor points near the interface, stars for vertical mesh segments, circles for horizontal mesh segments. Some are used for two different intersections. In* (b)*, we see selected complete stencils. The algorithm chooses a stencil for every point labeled by a circle or star in* (a)*.*

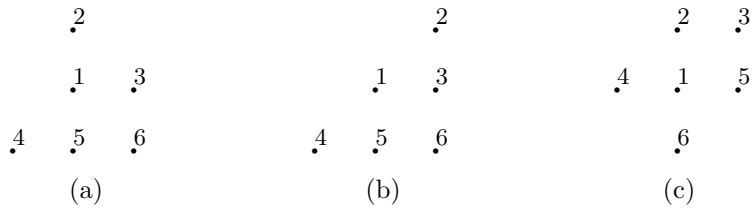

FIG. 3. *Three of the* 16 *possible stencils (the others are obtained by reflection and/or rotations by multiples of* $\pi/2$*) the algorithm allows for interpolation. Numbers indicate the row in* $\mathcal{P}$ *that corresponds to this stencil point and may be permuted in each figure. The anchor point is always the stencil point closest to the intersection.*

centered at these points contain $[0, h/2] \times [0, h/2]$. The constant $\sqrt{5/2}\,h$ is sharp because the disks of radius $\sqrt{5/2}\,h$ centered at $(h/2, -h/2)$ and $(h/2, h/2)$ contain only six grid points and have the point $(0, 0)$ on the boundary, so that disks of smaller radius have fewer than six points in them. ∎

The algorithm succeeds provided that the mesh size h is chosen small enough depending on the curvature of Γ and that the curve does not get "too close to itself" as expressed in the curve condition. If the program cannot find six points, it recommends a finer mesh. Up to symmetry (reflection and/or rotation by angles $\pi/2$, π, or $3\pi/2$), for closed curves only three constellations of the six points are allowed by the algorithm, shown in Figure 3. We find $\mathcal{P}$ using Cartesian coordinates centered at the anchor point, so that always $h_0 = k_0 = 0$ and all other h_i and k_j are integer multiples of h.

LEMMA 33. *The entries of* $\mathcal{P}^{-1}$ *as found by our algorithm are bounded as follows: entries in the first row* (*yield constant term in p*) *by* $O(h^0)$*, entries in the second and third row* (*linear terms*) *by* $O(h^{-1})$*, and entries in the last three rows* (*quadratic terms*) *by* $O(h^{-2})$*.*

Proof. We need to consider more than the three cases in Figure 3 since the anchor can be almost any of the points in each of the three allowed stencils, except the point labeled 1 in case (c). This gives 23 cases, up to row permutations and rotation of the stencils by multiples of $\pi/2$. In each of the 23 cases the matrix $\mathcal{P} = \mathcal{P}_1\mathcal{D}_h$ factors into

a matrix $\mathcal{P}_1$ which is independent of h with entries in $\{-2,-1,0,1,2\}$ and the same diagonal matrix $\mathcal{D}_h = \operatorname{diag}(1,h,h,h^2,h^2,h^2)$. $\mathcal{P}_1$ is invertible by Corollary 30, and the entries of the 23 possible inverses are bounded simply by the maximum absolute value over the 36×23 entries of the inverses, while $\mathcal{D}_h^{-1} = \operatorname{diag}(1,h^{-1},h^{-1},h^{-2},h^{-2},h^{-2})$. Finally, $\mathcal{P}^{-1} = \mathcal{D}_h^{-1}\mathcal{P}_1^{-1}$, which completes the proof. ∎

Now we describe how to compute one-sided limits: The goal is to estimate u^-, u_x^-, and u_{xx}^- on points in $\mathcal{I}$ that lie on horizontal mesh lines, and u^-, u_y^-, and u_{yy}^- on points in $\mathcal{I}$ that lie on vertical mesh lines.

Suppose the anchor point S for a fixed point $(x_t,y_t)\in\mathcal{I}$ has coordinates $(\bar{x},\bar{y})$, and the selected five neighbors have relative coordinates (h_j,k_j), $j=1,2,3,4,5$ (here $h_0=k_0=0$), where all six points lie on the "$-$" side of the interface. The restriction operator $R_S:\mathbf{R}^{(n_x-1)(n_y-1)}\to\mathbf{R}^6$ depends on S and restricts the values of any grid function z to the six points in the desired order. The quadratic polynomial p in shifted Cartesian coordinate variables $h=x-\bar{x}$ and $k=y-\bar{y}$ interpolates z on these six points, i.e.,

$$p(h_j,k_j) = p_0 + p_1h_j + p_2k_j + p_3h_j^2 + p_4h_jk_j + p_5k_j^2 = (R_Sz)_j\,.$$

As in Lemma 28 we know that $[p_0,p_1,p_2,p_3,p_4,p_5]^T = \mathcal{P}_S^{-1}R_Sz$.

THEOREM 34. *If we set $h^-\equiv\bar{x}-x_t$ and $k^-\equiv\bar{y}-y_t$, and let $z=Eu$, then*

$$\begin{aligned}
u^-(x_t,y_t) &= p(-h^-,-k^-)+O(h^3) = p_0 - p_1h^- - p_2k^- + p_3(h^-)^2 \\
&\qquad + p_4h^-k^- + p_5(k^-)^2 + O(h^3),\\
u_x^-(x_t,y_t) &= \frac{\partial p}{\partial h}(-h^-,-k^-)+O(h^2) = p_1 - 2p_3h^- - p_4k^- + O(h^2),\\
u_{xx}^-(x_t,y_t) &= \frac{\partial^2 p}{\partial h^2}(-h^-,-k^-)+O(h) = 2p_3 + O(h),\\
u_y^-(x_t,y_t) &= \frac{\partial p}{\partial k}(-h^-,-k^-)+O(h^2) = p_2 - p_4h^- - 2p_5k^- + O(h^2),\\
u_{yy}^-(x_t,y_t) &= \frac{\partial^2 p}{\partial k^2}(-h^-,-k^-)+O(h) = 2p_5 + O(h).
\end{aligned}$$

Proof. Use Taylor expansions about the anchor point. Minus signs result from our convention to define h^- as subtracting an interface coordinate from a grid coordinate, i.e., the expansion about (x_t,y_t) instead of $(\bar{x},\bar{y})$. ∎

REMARK 35. *By Lemma* 33 *the constants in the order terms in Theorem* 34 do not depend on the interface geometry. *Also, the constants* do not depend on the coefficients of the equation, *other than implicitly through the bounds on derivatives of* u.

Written as linear operators applied to Eu,

$$\begin{aligned}
u^- &\approx \left[1,-h^-,-k^-,h^{-2},h^-k^-,k^{-2}\right]\mathcal{P}_S^{-1}R_SEu,\\
u_x^- &\approx \left[0,1,0,-2h^-,-k^-,0\right]\mathcal{P}_S^{-1}R_SEu,\\
u_{xx}^- &\approx [0,0,0,2,0,0]\,\mathcal{P}_S^{-1}R_SEu,\\
u_y^- &\approx \left[0,0,1,0,-h^-,-2k^-\right]\mathcal{P}_S^{-1}R_SEu,\\
u_{yy}^- &\approx [0,0,0,0,0,2]\,\mathcal{P}_S^{-1}R_SEu.
\end{aligned}$$

By applying these discrete linear operators to U instead of Eu, composing with coordinate transformations (see section 5) as needed and finally taking linear

combinations as imposed by the jump conditions (see section 4), we know how to discretize the jump conditions in section 4. For example, we discretize

$$[u_\xi] = \frac{\tilde{v}}{\beta^+} + (\rho - 1)u_\xi^- \tag{47}$$

as

$$[u_\xi] \approx f_2 + (\rho - 1)\begin{pmatrix} c & s \end{pmatrix}\begin{pmatrix} 0 & 1 & 0 & -2h^- & -k^- & 0 \\ 0 & 0 & 1 & 0 & -h^- & -2k^- \end{pmatrix}\mathcal{P}_S^{-1}R_S E u,$$

where $f_2 = \tilde{v}/\beta^+$. All the linear operations are combined into one linear operator D, whose columns correspond to grid points (it has six nonzero entries per row) and whose rows are ordered like the jump variables. The discretization of all jump conditions is

$$C = F_2 - D^T U.$$

We can combine the discretization of the PDE (45) and the discretization of the jump conditions:

$$\begin{aligned} \Delta_h U - \Psi C &= F_1, \\ D^T U + C &= F_2. \end{aligned} \tag{48}$$

This notation covers Problems (a), (b), and (c) for piecewise constant coefficients. F_1, F_2, and D^T depend on the problem, but even $\mathcal{P}_S^{-1}$ and R_S, two important factors of D^T, depend only on the interface and mesh geometry. Multiple interfaces are handled by simply stacking the D^T matrices and jump vectors C and concatenating the Ψ matrices, even if the jump conditions are different for the different interfaces. In case (a), simply $D^T = 0$ and F_2 contains the signed magnitudes of the jumps in the coordinate directions. We define the jump truncation error to measure how well the jumps in u and derivatives satisfy the discrete jump equations, and observe that it is trivially zero for Problem (a).

For Problems (b) and (c), with the operators we have given above (i.e., for a six point stencil), it is easy to see that for nonzero rows in D^T the jump truncation error is $O(h^3)$ for entries in C approximating $[u]$, $O(h^2)$ for entries in C approximating $[u_x]$ and $[u_y]$, and $O(h)$ for entries in C approximating $[u_{xx}]$ and $[u_{yy}]$. Checking carefully the magnitudes of the coefficients in Ψ that multiply these terms (compare Lemma 33) we see that after elimination of C the first equation has truncation error $O(h^2)$ except at neighbors of the interface, where the truncation error is $O(h)$. The bounds in these estimates depend on the contrast in the coefficient, but not on the geometry; this property was not available for the original IIM [4].

6.3. Solving the linear systems. Equation (45) with known C can be efficiently solved for U since Δ_h^{-1} is easily applied to a vector via a fast Poisson solver; see, for example, [13]. We take advantage of this by looking at the second Schur-complement of the 2×2 block system (48),

$$\left(I + D^T \Delta_h^{-1} \Psi\right) C = F_2 - D^T \Delta_h^{-1} F_1. \tag{49}$$

The similarity of this equation with the boundary integral equations of potential theory (see [16]) may provide the insights needed to prove the stability of this approach in the future, while here we only verify convergence numerically. The entries in C

correspond to double and single layer densities. Ψ discretizes their influence on the domain, i.e., it resembles a delta or dipole. Δ_h^{-1} is a discrete Green's kernel for the rectangle, and D^T corresponds to restricting u and derivatives to the interface. Finally, (49) resembles a Fredholm equation of the second kind along the interface. Once C is found, it takes one more solution of the first equation in (48) to find U.

Equation (49) is best solved with an iterative method (we use GMRES from [3]; see [12]) to avoid forming the matrix on the left explicitly. The main cost per iteration lies in finding $\Delta_h^{-1}(\Psi C)$ and is $O(n_x n_y \log(n_x n_y))$. In order to use direct methods on (49) one would need an explicit formula for Δ_h^{-1}. One way to achieve this was suggested by Proskurowski and Widlund in [11], where a different choice of basic problem on the rectangle, namely periodic boundary conditions, allows cheap computation of the replacement of Δ_h^{-1} in that setting. This in turn allows forming the "small" matrix on the left in (49) explicitly and brings down the cost per iteration to $O(m^2)$.

7. Computational examples. In all examples below, the computational domain Ω is a square, so that $n_x = n_y = n$. E_n denotes the vector of errors at the grid points; T_n is the usual truncation error (for (45) only). For discretization with $n-1$ by $n-1$ interior points, by the ratio $\div$ we mean

$$\frac{\|E_n\|_\infty}{\|E_{n/2}\|_\infty} \quad \text{or} \quad \frac{\|T_n\|_\infty}{\|T_{n/2}\|_\infty}.$$

For computational purposes, the interfaces are assumed to be cubic spline interpolants of given points on the interface. Forces at the interface are also assumed to be specified at these points. All other needed quantities are interpolated from these using periodic cubic splines; for details, see [16].

In all but example 7.2 (b), we have chosen enough points on the interfaces so that the influence of an inexact interface representation may be neglected.

7.1. Singular sources. This example is interesting because it demonstrates Theorem 26 numerically and shows how EJIIM compares with IIM [4] for a problem of type (a). Let

$$u(x,y) = \begin{cases} 1 & \text{for } (r,\alpha) \in \Omega^- = \{(x,y) \in [0,2]\times[0,2] | r < s\}, \\ 1 - \log(r/s) & \text{for } (r,\alpha) \in \Omega^+ = \{(x,y) \in [0,2]\times[0,2] | r > s\}, \end{cases}$$

where s is the radius of a circular interface. Here $r = \sqrt{(x-1)^2 + (y-1)^2}$ and $\alpha = \arctan((y-1)/(x-1))$ are polar coordinates centered at $(1,1)$. Then u satisfies $\Delta u = 0$ with $[u] = 0$ and $[u_n] = -1/s$. This example is adapted from [4].

Table 1 shows the results of the computations for (29) with the above jumps and $s = 0.5$, compared with numbers from [4]. The boundary data are found by evaluating the analytic solutions. We see that for a given mesh, our method without (EJIIM, columns 4, 5) or with (EJIIM-2, columns 6, 7) the third order corrections give more accurate answers than the IIM (columns 2, 3). By including the third order corrections, we reduce the truncation error by one order of magnitude—compare columns 9 and 11, which give the ratios between consecutive truncation errors, and Figure 4(b) and Figure 5(a). This does not improve the error in the max norm, but yields a smoother error as can be seen comparing Figure 4(c) and Figure 5(b).

All methods converge with $O(h^2)$ and perform better on the coarsest mesh than Peskin's IBM on the finest mesh as reported in [4] for this problem.

TABLE 1
Numerical results for a singular source term.

	IIM		EJIIM		EJIIM-2		EJIIM		EJIIM-2	
n	$\|E_n\|_\infty$	$\div$	$\|E_n\|_\infty$	$\div$	$\|E_n\|_\infty$	$\div$	$\|T_n\|_\infty$	$\div$	$\|T_n\|_\infty$	$\div$
20	2.4e-3		1.4e-3		1.3e-3		2.8e-1		1.1e-1	
40	8.4e-4	2.9	1.8e-4	7.7	2.7e-4	4.9	1.6e-1	1.8	3.0e-2	3.7
80	2.5e-4	3.4	6.6e-5	2.7	7.4e-5	3.7	8.2e-2	1.9	8.9e-3	3.4
160	6.7e-5	3.7	1.9e-5	3.4	1.9e-5	3.9	4.2e-2	2.0	2.3e-3	3.9
320	1.6e-5	4.3	3.4e-6	5.7	4.8e-6	4.0	2.1e-2	2.0	6.6e-4	3.6

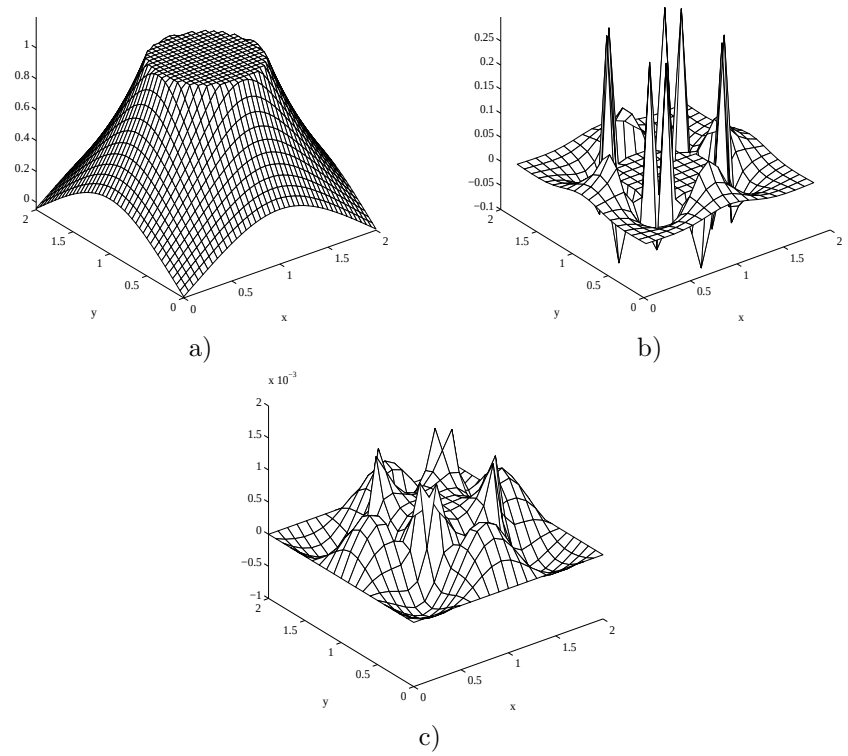

FIG. 4. (a) *Exact solution for Example* 7.1 *on a* 40×40 *mesh.* (b) *Truncation error and* (c) *error in the computed solution for EJIIM on Example* 7.1 *without third order corrections. The truncation error is only defined in the interior, while the error on the boundary is zero due to the exact boundary conditions. The spikes in* (b) *are terms of magnitude* $O(h)$*; they get smoothed out to* $O(h^2)$ *in* (c).

7.2. Dirichlet BVPs. These examples are interesting because they demonstrate how EJIIM can handle Dirchlet BVP of different types. The IIM [4] did not cover BVP on irregular domains, but was adapted by Yang [18] to this case.

(a) Consider the "exterior" Dirichlet BVP, $\Delta u = 0$, $u = 0$ on $\partial\Omega$, and $u = 1$ on Γ given in polar coordinates centered at $(0.5, 0.5)$ by $r(\theta) = 0.25 + 0.05\sin(6\theta)$, $\theta \in [0, 2\pi]$. The solution is extended to be 1 in Ω^- (so $[u] = 0$) with differences enforcing this value on all interior neighbors of Γ; see Figure 6(a). Table 2 shows how the number m of interior neighbors of the interface increases with the number n of mesh points, while the number of GMRES iterations grows slowly. For $n = 20$,

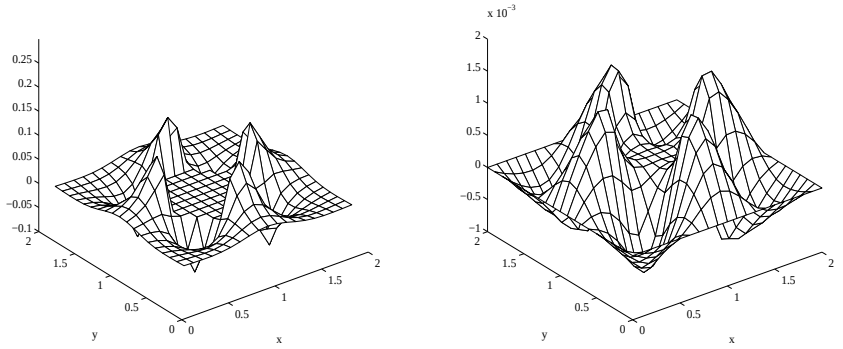

FIG. 5. *Truncation error* (a) *and error in the computed solution* (b) *for EJIIM for Example* 7.1 *including third order corrections. The spikes have disappeared, and the truncation error is smooth in the tangential direction on either side of the interface.*

TABLE 2
Numerical results for "exterior" Dirichlet BVP.

n	m	its	Flops	CPU″
40	72	36	3.0e+07	2.7e+01
80	146	47	1.7e+08	5.8e+01
160	292	63	1.0e+09	1.8e+02
320	586	83	5.9e+09	7.5e+02

the mesh did not resolve the interface well enough for one-sided differences. In the future we want to keep the number of iterations constant by reducing the number of auxiliary variables, similar to [6]. The CPU timings are included merely to illustrate the fact that at least medium size problems can be set up and solved efficiently.

(b) Consider the "interior" BVP: $\Delta u + \kappa u = f$ where $u(x,y) = 2(x-0.7)^2 + 2(y-0.4)^2$, $\kappa(x,y) = 12((x-0.2)^2 + (y+0.1)^2)/(2 + (x-0.2)^4 + (y+0.1)^4)$, and f satisfies the equation. This variable coefficient Helmholtz equation is solved with Dirichlet boundary condition given by the exact solution on $\partial\Omega^-$, which is given by $r(\theta) = 0.395 + 0.05\sin(6\theta)$ in polar coordinates centered at $(0.5, 0.5)$. The solution (see Figure 6(b)) is found on a Cartesian grid with jump conditions of the form in problem section 4.2(b), using GMRES on a preconditioned system similar to (56) below. The solution is a second-degree polynomial and should be reproduced exactly up to machine precision by our second-order method. This is not the case only because the representation of the interface is not exact. Figure 6(c) shows the error in the case that the interface is given by 101 points. Table 3 shows how the error behaves when the representation of the interface is improved; we see at least fourth order behavior which should not come as a surprise given the quality of interpolation by cubic splines. In the table, n_1 is the number of points on the interface. The points are equally spaced in θ which gives a slight advantage over equal spacing in arclength since parts of the curve with high curvature receive more points.

7.3. Composite material problem. This example is interesting because it shows how EJIIM compares with FIIIM [6] for problems of type (c) with piecewise constant coefficients. For large contrast in material properties, it can be crucial to do

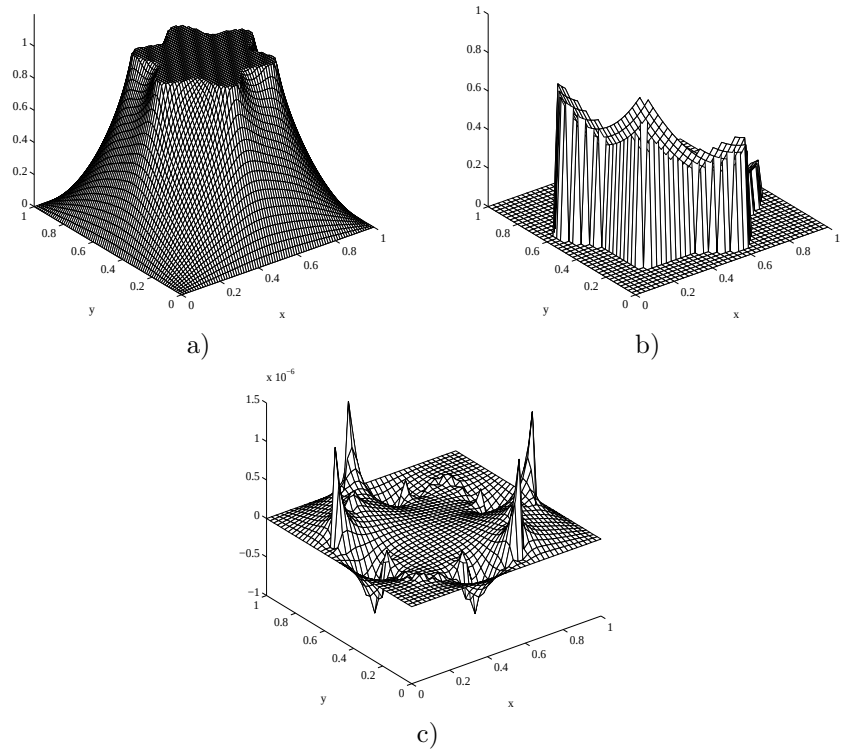

FIG. 6. (a) *Solution for Example* 7.2 (a)*, computed on a* 80×80 *mesh.* (b) *Solution for Example* 7.2 (b) *computed on a* 40×40 *mesh. Values outside* Ω^- *are part of the solution; they are all very close to zero as they should be by our ansatz.* (c) *Error for* 101 *control points on the interface.*

TABLE 3
Numerical results for "interior" Dirichlet BVP.

n	n_1	$\|E_n\|_\infty$	$\div$
40	51	4.5e-5	
40	101	1.3e-6	35
40	201	3.2e-8	41
40	401	2.3e-9	14

the one-sided interpolations on the correct side of the interface. Let

$$u^-(r,\alpha) = \frac{2r\cos\alpha}{\rho+1+s^2(\rho-1)},$$
$$u^+(r,\alpha) = \frac{(r(\rho+1)-s^2r^{-1}(\rho-1))\cos\alpha}{\rho+1+s^2(\rho-1)},$$

$$u(x,y) = \begin{cases} u^-(r,\alpha) & \text{for } (r,\alpha)\in\Omega^- = \{(x,y)\in[0,1]\times[0,1] | r<s\} \\ u^+(r,\alpha) & \text{for } (r,\alpha)\in\Omega^+ = \{(x,y)\in[0,1]\times[0,1] | r>s\}, \end{cases}$$

where s is the radius of the circular interface. Here $r=\sqrt{(x-0.5)^2+(y-0.5)^2}$ and $\alpha = \arctan((y-0.5)/(x-0.5))$ are polar coordinates centered at $(0.5, 0.5)$. Then u

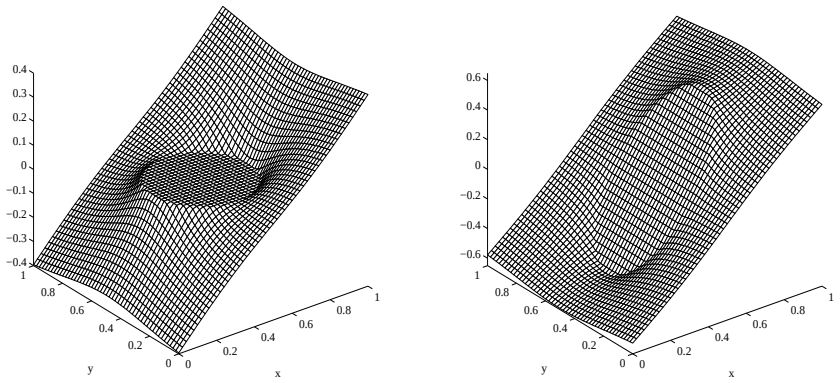

FIG. 7. *Exact solutions for Example* 7.3. *In* (a)*, we see the solution for* $\rho = 5000$*, in* (b) *we see the solution for* $\rho = 1/5000$*. In both cases, the boundary data are found by evaluating the analytic solutions.*

TABLE 4
Results for Example 7.3 *with* $\rho = 5000$.

	FIIIM		Interior EJIIM				Exterior EJIIM			
n	$\|E_n\|_\infty$	$\div$	$\|E_n\|_\infty$	$\div$	$\|T_n\|_\infty$	$\div$	$\|E_n\|_\infty$	$\div$	$\|T_n\|_\infty$	$\div$
25	1.2e−2		1.4e−3		1.0e+0		9.1e−2		1.4e+1	
50	9.2e−2	0.1	3.5e−4	4.0	1.5e+0	0.7	2.5e−2	3.7	1.1e+1	1.3
100	5.9e−2	1.5	9.0e−5	3.9	9.8e−1	1.5	6.8e−3	3.7	4.5e+0	2.4
200	7.7e−3	7.7	2.2e−5	4.1	5.0e−1	1.9	2.0e−3	3.5	3.7e+0	1.2

TABLE 5
Results for Example 7.3 *with* $\rho = 1/5000$.

	FIIIM		Interior EJIIM				Exterior EJIIM			
n	$\|E_n\|_\infty$	$\div$	$\|E_n\|_\infty$	$\div$	$\|T_n\|_\infty$	$\div$	$\|E_n\|_\infty$	$\div$	$\|T_n\|_\infty$	$\div$
25	5.2e−3		1.9e−3		1.2e+0		1.3e+1		8.0e+4	
50	1.6e−3	3.3	5.5e−4	3.4	1.7e+0	0.7	5.6e+0	2.4	5.9e+4	1.4
100	2.3e−4	6.8	1.3e−4	4.2	1.1e+0	1.5	6.4e−1	8.8	2.6e+4	2.3
200	5.0e−5	4.6	3.2e−5	4.1	5.7e−1	1.9	8.1e−2	7.8	2.2e+4	1.2

satisfies $\Delta u = 0$ with $[u] = 0$ and $u_n^+ = \rho u_n^-$ at the interface $r = s$. This is a special case of a general analytic solution for circular interfaces found in [14]. Figure 7 shows the exact solutions on the square $[0,1] \times [0,1]$ for $\rho = 5000$ and $\rho = 1/5000$, with $s = 0.25$ in both cases.

Tables 4 and 5 show the error in the infinity norm for FIIIM [6], EJIIM with jump approximations based on interior points, and EJIIM with jump approximations based on exterior points for these two problems, where the boundary values on the square are found by evaluating the analytic solutions.

The solution computed by FIIIM for the first problem ($\rho = 5000$) on the finest mesh is good, but the behavior on the coarser meshes does not allow us to deduce this fact. For the second problem ($\rho = 1/5000$), FIIIM converges well with second order. EJIIM based on interior points performs extremely well for both examples and in particular converges with second order. For the first problem, the solution found *on the coarsest mesh* is better than the approximations on the finest meshes found by the other two methods. EJIIM with jump approximations in the exterior performs

well for the first example and poorly (in terms of error magnitude) for the second.

This may be explained by looking at the truncation error. In Ω^-, u is planar in both cases: the interior finite differences for the normal derivatives are exact, the jump corrections are exact, and the truncation error results purely from the discretization of the PDE, which is confirmed by comparing the truncation errors for interior differences in column 6 in Tables 4 and 5. In Ω^+, u varies mildly but the third derivatives do not vanish. In the first problem, the exterior differences are multiplied with a factor $1/5000 - 1$ while in the second problem the factor is $5000 - 1$. Note that the ρ used in the definition of u is exactly the factor $\rho = \beta^-/\beta^+$ entering the interior differences in (42), while for exterior differences the meaning of ρ is reciprocal.

7.4. Variable discontinuous coefficients. Again we compare our results with the IIM on an example from [4]. Let $r^2 = x^2 + y^2$ and

$$\nabla \cdot (\beta \nabla u) = f + C \int_\Gamma \delta(\vec{x} - \vec{X}(\vec{y}))d\sigma(\vec{y}), \tag{50}$$

$$f(x, y) = 8r^2 + 4, \tag{51}$$

$$\beta(x, y) = \begin{cases} r^2 + 1 & \text{if } r \le 0.5, \\ b & \text{if } r > 0.5. \end{cases} \tag{52}$$

Dirichlet boundary conditions are determined from the exact solution,

$$u(x, y) = \begin{cases} r^2 & \text{if } r < 0.5, \\ \left(1 - \frac{9}{8b}\right)/4 + \left(r^4 + 2r^2\right)/(2b) + C\log(2r)/b & \text{if } r > 0.5. \end{cases} \tag{53}$$

The two parameters b and C may be chosen arbitrarily. The jump conditions (44) simplify significantly, but we need to take care of the case $C \neq 0$, where the jumps are as follows:

$$[\tilde{u}] = \left(\frac{2\sqrt{b}}{\sqrt{5}} - 1\right)\tilde{u}^-,$$

$$[\tilde{u}_\xi] = \left(\frac{\sqrt{5}}{2\sqrt{b}} - 1\right)\tilde{u}^-_\xi - \frac{\sqrt{5}}{5\sqrt{b}}\tilde{u}^- + \frac{2C}{\sqrt{b}},$$

$$[\tilde{u}_\eta] = \left(\frac{2\sqrt{b}}{\sqrt{5}} - 1\right)\tilde{u}^-_\eta,$$

$$[\tilde{u}_{\eta\eta}] = \left(\frac{\sqrt{5}}{\sqrt{b}} - \frac{4\sqrt{b}}{\sqrt{5}}\right)\tilde{u}^-_\xi - \frac{2\sqrt{5}}{5\sqrt{b}}\tilde{u}^- + \left(\frac{2\sqrt{b}}{\sqrt{5}} - 1\right)\tilde{u}^-_{\eta\eta} + \frac{4C}{\sqrt{b}},$$

$$[\tilde{u}_{\xi\eta}] = \left(\frac{6\sqrt{5}}{\sqrt{b}} - \frac{4\sqrt{b}}{\sqrt{5}}\right)\tilde{u}^-_\eta + \left(\frac{\sqrt{5}}{2\sqrt{b}} - 1\right)\tilde{u}^-_{\eta\xi},$$

$$[\tilde{u}_{\xi\xi}] = \left(\frac{4\sqrt{b}}{\sqrt{5}} - \frac{\sqrt{5}}{\sqrt{b}}\right)\tilde{u}^-_\xi + \left(\frac{2\sqrt{5}}{5\sqrt{b}} - \frac{36}{25}\right)\tilde{u}^- - \left(\frac{2\sqrt{b}}{\sqrt{5}} - 1\right)\tilde{u}^-_{\eta\eta} - \frac{4C - 6}{\sqrt{b}} - \frac{12\sqrt{5}}{5}.$$

The behavior for extreme values of b is of interest, but [4] only provides data for the cases $b \in \{10, -3\}$ and $C = 0.1$. The solutions for these two cases are shown in Figure 8. For $b < 0$, the Liouville transform may also be applied, after multiplying the equation by -1 on Ω^- in order to be able to take $\sqrt{\beta}$. This requires

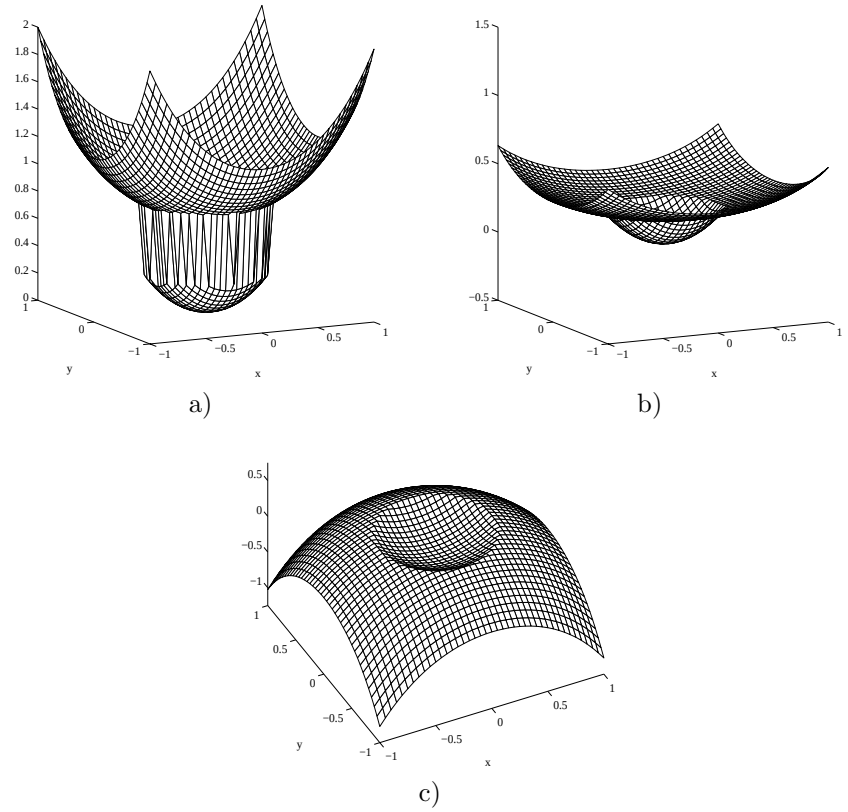

FIG. 8. (a) *Solution $\tilde{u}$ for Example* 7.4 *with $b = 10$, computed on a 40×40 mesh.* (b) *Solution u for $b = 10$.* (c) *Solution u for $b = -3$.*

TABLE 6
Results for Example 7.4 *with $b = 10$, $C = 0.1$.*

	IIM		EJIIM (u)		Liouville ($\tilde{u}$)		Liouville		GMRES
n	$\|E_n\|_\infty$	$\div$	$\|E_n\|_\infty$	$\div$	$\|E_n\|_\infty$	$\div$	$\|T_n\|_\infty$	$\div$	iterations
20	3.5e-3		7.6e-4		1.4e-3		3.4e-1		10
40	7.6e-4	4.7	2.4e-4	3.2	7.5e-4	1.8	4.0e-1	0.9	10
80	1.7e-4	4.6	7.9e-5	3.0	2.5e-4	3.0	2.6e-1	1.5	9
160	3.6e-5	4.6	2.2e-5	3.6	6.9e-5	3.6	1.4e-1	1.9	9
320	8.4e-6	4.3	5.3e-6	4.2	1.7e-5	4.1	9.2e-2	1.5	8

the following replacements in the jump equations: $C \to -C$, $\rho^{1/2} \to -\rho^{1/2}$, and $[(\sqrt{\beta})_\xi]/\sqrt{\beta^+} \to -[(\sqrt{\beta})_\xi]/\sqrt{\beta^+}$. Finally, f^+ changes sign and affects one of the constant terms. Table 6 shows the results from [4] and for our method for $b = 10$ and $C = 0.1$. Both methods converge quadratically, but EJIIM gives better results particularly on the coarser grids. To demonstrate the efficiency of our method, we also include the number of iterations that GMRES needs to solve the large linear systems for this problem. Similar to (48), now

$$\begin{aligned} (\Delta_h + K)\,\tilde{U} &= F_1 + \Psi C, \\ C &= F_2 - D^T \tilde{U}, \end{aligned} \tag{54}$$

where K is a diagonal matrix with entries $\Delta(\sqrt{\beta})(x_i, y_j)/\sqrt{\beta}(x_i, y_j)$. Instead of using

TABLE 7
Results for Example 7.4 *with* $b = -3$, $C = 0.1$.

	EJIIM (u)		Liouville ($\tilde{u}$)		Liouville		GMRES
n	$\|E_n\|_\infty$	÷	$\|E_n\|_\infty$	÷	$\|T_n\|_\infty$	÷	iterations
20	8.6e-3		1.4e-2		4.0e-1		10
40	3.0e-3	2.9	5.2e-3	2.7	5.1e-1	0.8	13
80	8.8e-4	3.4	1.5e-3	3.5	3.4e-1	1.5	12
160	2.4e-4	3.7	4.2e-4	3.6	1.9e-1	1.8	11
320	6.3e-5	3.8	1.1e-4	3.8	1.1e-1	1.7	10

a fast solver for the variable Helmholtz equation, we eliminate the second equation and work with the bigger Schur-complement,

$$\left(\Delta_h + K + \Psi D^T\right)\tilde{U} = F_1 + \Psi F_2, \tag{55}$$

and after preconditioning

$$\left(I + \Delta_h^{-1}\left(K + \Psi D^T\right)\right)\tilde{U} = \Delta_h^{-1}\left(F_1 + \Psi F_2\right). \tag{56}$$

Using GMRES lets us avoid forming the matrix on the left. From the results for $b = -3$ in Table 7, we see again that the number of iterations is fairly independent of the problem size and rather low.

The simple geometry and radial shape of β and u may account for some of this good performance, and further testing on more general geometries and coefficients is planned.

7.5. Groundwater flow problem. These examples are of interest because they combine three (two) different interface conditions. We consider an equation for the pressure in a problem of (steady) groundwater flow, as previously studied by Yang [18]. Included in the computational domain are one more permeable object and one less permeable object, modeled by discontinuous β with interior differences, and two impermeable objects, modeled by the Neumann boundary condition $u_n^- = 0$. See Figure 9 for the geometry of the interfaces. For the jumps across $\partial\Omega_2^+$ and $\partial\Omega_4^+$, we use interior differences (motivated by the results in section 7.3), while for jumps across $\partial\Omega_1^+$ and $\partial\Omega_3^+$ we have to use exterior differences. For exterior differences to work, interfaces have to be sufficiently far apart. At the top and bottom boundaries, we impose $u_y = 0$. These boundaries are treated via Schur-complements as well to make use of a fast Poisson solver. On the left and right boundaries, the pressure is at two different constants.

A numerical solution is plotted in Figure 10(a). The jump condition $[u] = -u^-$ sets up a Dirichlet problem inside the impermeable objects, with boundary condition zero, hence solution zero. Figure 10(a) demonstrates that this is approximately the case.

In our setup different conditions for different interfaces can be incorporated by simply stacking the sparse matrices. In Figure 10(b), we see the sparsity pattern of the matrix in system (48). The bottom left contains the entries for D, with distinct entries for the two boundaries with Neumann boundary conditions and the four objects. On the top right we see the entries of Ψ, the discretization of the deltas (for permeable objects) and dipoles (for impermeable objects).

The stacking can be carried out to a much higher degree than in Figure 10. Figure 11 shows an example with 25 included objects, and we have successfully carried out experiments with up to 1985 circular objects on a 256×256 mesh.

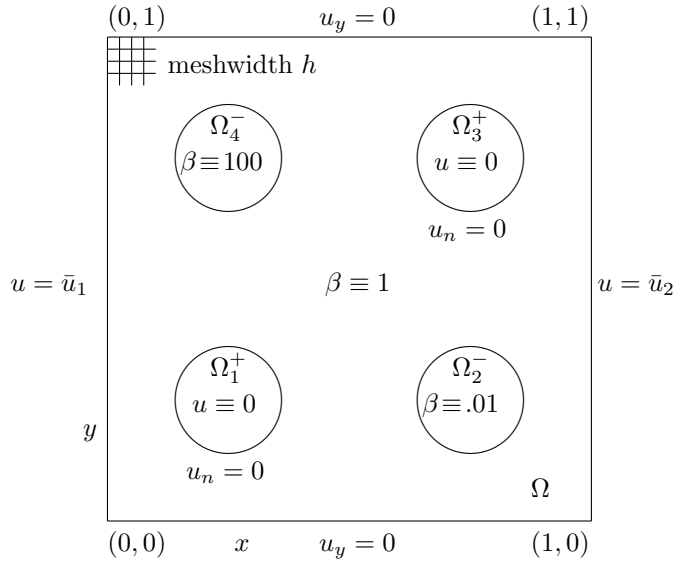

FIG. 9. *The geometry of the first groundwater flow problem in section* 7.5 : *One object of higher permeability* Ω_4*, one object of lower permeability* Ω_2*, and two impermeable objects* Ω_1 *and* Ω_3*. Dirichlet boundary conditions on* $x = 0$*,* $x = 1$ *and Neumann boundary conditions at* $y = 0$ *and* $y = 1$*. Superscript "−" indicates that differences are done in the interior domain for the interface given by the boundary of the object. This is impossible for impermeable objects; they need to be modeled by exterior differences.*

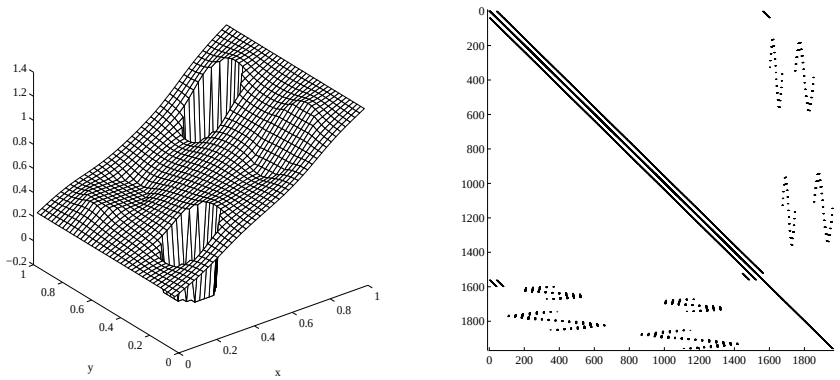

FIG. 10. *Computed solution and sparsity structure of the system in Example* 7.5 *with four included objects. In* (a)*, we see more uniform pressure in regions of higher permeability, while the behavior near regions of low permeability is very similar to the behavior near impermeable objects. Inside the impermeable objects, the numerical solution is very close to zero as it should be by our ansatz. In* (b)*, six different interfaces can be distinguished: two Neumann boundary conditions, two permeable objects with interior differences, and two nonpermeable objects with exterior differences. Standard ordering of the mesh variables and sorting the intersections with arclength yields patterns that "resemble" the interfaces.*

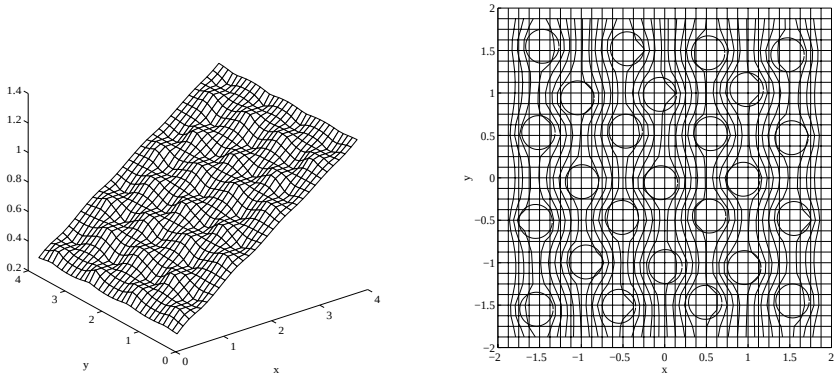

FIG. 11. (a) *Computed solution and* (b) *mesh, interfaces, and contour lines for a problem with* 25 *objects of very high contrast* (1000). *We impose Dirichlet boundary conditions on the right and left boundaries, and Neumann boundary conditions on the top and bottom boundaries.*

8. Conclusion. We have proven convergence of the EJIIM for a simple case of an equation in one dimension with solution dependent jumps, and for an equation with known jumps in two dimensions. From a practical viewpoint, there are several nice features of the EJIIM approach. We work with sparse matrices and at every iteration solve a standard Poisson problem on a rectangle, a problem for which fast solvers abound. Multiple interfaces, with varying boundary conditions, are covered by simply "stacking" their matrix representations. The finite difference corrections extend to the discretization of many partial (and ordinary) differential equations, including nonlinear equations, in a more straightforward way than in [17]. EJIIM requires only that formulas for the discontinuities across the interface can be written depending only on solution values on one side of the interface. The deep connections with potential theory still to be explored were hinted at by similarity with capacitance methods; see [18] and [11]. In summary, EJIIM allows some theory and works great in practice as we have seen in the last section, and in particular improves on the performance by its predecessors, Peskin's IBM [10, 15], Li and LeVeque's IIM [4, 5], and Li's FIIIM [6].

Acknowledgments. We would like to thank Randall J. LeVeque and Zhilin Li for encouraging us to participate in the development of the IIM and to thank Zhilin Li for making his computer codes available to us. Andreas Wiegmann enjoyed insightful comments on the presentation of EJIIM by David Adalsteinsson.

REFERENCES

[1] R. P. BEYER AND R. J. LEVEQUE, *Analysis of a one-dimensional model for the immersed boundary method*, SIAM J. Numer. Anal., 29 (1992), pp. 332–364.

[2] G. H. GOLUB AND C. F. VAN LOAN, *Matrix Computations*, 2nd ed., The Johns Hopkins University Press, Baltimore, MD, 1989.

[3] C. T. KELLEY, *Iterative Methods for Linear and Nonlinear Equations*, Frontiers in Appl. Math. 16, SIAM, Philadelphia, PA, 1995.

[4] R. J. LEVEQUE AND Z. L. LI, *The immersed interface method for elliptic equations with discontinuous coefficients and singular sources*, SIAM J. Numer. Anal., 31 (1994), pp. 1019–1044.

[5] Z. LI, *The Immersed Interface Method: A Numerical Approach to Partial Differential Equations with Interfaces*, Ph.D. thesis, Department of Applied Mathematics, University of

Washington, Seattle, WA, 1994.

[6] Z. Li, *A fast iterative algorithm for elliptic interface problems*, SIAM J. Numer. Anal., 35 (1998), pp. 230–254.

[7] R. A. Lorentz, *Multivariate Birkhoff Interpolation*, Springer-Verlag, New York, 1992.

[8] A. Mayo, *The fast solution of Poisson's and the biharmonic equations on irregular regions*, SIAM J. Numer. Anal., 21 (1984), pp. 285–299.

[9] K. W. Morton and D. F. Mayers, *Numerical Solution of Partial Differential Equations*, Cambridge University Press, New York, 1994.

[10] C. S. Peskin, *Lectures on Mathematical Aspects of Physiology*, Lectures in Appl. Math. 19, AMS, Providence, RI, 1981.

[11] W. Proskurowski and O. Widlund, *On the numerical solution of Helmholtz's equation by the capacitance matrix method*, Math. Comp., 30 (1976), pp. 433–468.

[12] Y. Saad and M. H. Schultz, *GMRES: A generalized minimal residual algorithm for solving nonsymmetric linear systems*, SIAM J. Sci. Statist. Comput., 7 (1986), pp. 856–869.

[13] P. N. Swarztrauber, *Fast Poisson solvers*, in Studies in Numerical Analysis, G. H. Golub, ed., Studies in Mathematics 24, Mathematical Association of America, Washington, DC, 1984.

[14] C. F. Tolmasky and A. Wiegmann, *Recovery of small perturbations of an interface for an elliptic inverse problem via linearization*, Inverse Problems, 15 (1999), pp. 465–487.

[15] C. Tu and C. S. Peskin, *Stability and instability in the computation of flows with moving immersed boundaries: A comparison of three methods*, SIAM J. Sci. Statist. Comput., 13 (1992), pp. 1361–1376.

[16] A. Wiegmann, *The Explicit Jump Immersed Interface Method and Interface Problems for Differential Equations*, Ph.D. thesis, Department of Mathematics, University of Washington, Seattle, WA, 1998.

[17] A. Wiegmann and K. P. Bube, *The immersed interface method for nonlinear differential equations with discontinuous coefficients and singular sources*, SIAM J. Numer. Anal., 35 (1998), pp. 177–200.

[18] Z. Yang, *A Cartesian Grid Method for Elliptic Boundary Value Problems in Irregular Regions*, Ph.D. thesis, Department of Applied Mathematics, University of Washington, Seattle, WA, 1996.